11-15-2012

Design and Synthesis of Fluorescence Turn-on Probes for Iron

Randy K. Jackson
University of Connecticut - Storrs, j.randy@sbcglobal.net

Design and Synthesis of Fluorescence Turn-on Probes for Iron

Randy K. Jackson

B.A., Hunter College of CUNY, 2004

A Thesis

Submitted in Partial Fulfillment of the

Requirements for the Degree of

Master of Science

At the

University of Connecticut

2012

APPROVAL PAGE

Masters of Science Thesis

Design and Synthesis of Fluorescence Turn-on Probes for Iron

Presented by

Randy K. Jackson, B.A.

Major Advisor_____
Dr. Christian Brückner

Associate Advisor_____
Dr. Amy Howell

Associate Advisor_____
Dr. James Stuart

University of Connecticut

2012

Acknowledgements

There are a number of people whom have helped me during pursuit of my graduate education. I am especially grateful to my parents, Lawrence and Cheryl Jackson, brother, Atiba for providing love and encouragement. Because of their support, I was able to persevere when the going got tough. Special thanks also go out to Sherwayne, Ron, my aunts, uncles, and cousins for supporting me on this journey. I am forever indebted to my late grandparents, James and Sheila Rankin for instilling in me at a young age the values and virtues that are very much a part of my adult life.

I would also like to thank Dr. Shawn Burdette for providing guidance on the research projects that I worked on. It was a pleasure working in the field of fluorescence turn-on sensors and azobenzene photochemistry. I particularly enjoyed the stimulating discussions on photophysics with Dan and would also like thank to Hannah, Dhammika and Celina for their contributions to problem solving, support and friendship.

Other members of the UCONN chemistry department also played key roles in my success. I would like to thank Emilie Hogrebe for answering all of my questions and being very approachable, as well as Osker Dahabsu, Ashley Butler and Charlene Fuller for their help. I would also like to acknowledge the support received from Dr. Martha Morton who was always available to answer all of my questions on NMR spectroscopy and Dr. You-Jun for also being very helpful in obtaining mass spectrometry data.

An Infinite amount of gratitude is also extended to Drs. Amy Howell, Christian Brückner, and James Stuart for being on my committee and also helping with providing solutions to problems that I encountered. I am also grateful to the following funding

sources that made my academic pursuits possible: The UCONN Research Foundation, Multicultural Scholars Fellowship and the CURE/CBIA awards fellowship.

Last but not least I would like to thank Susan for her encouragement and for standing by me. Thanks to Josh, Naf, King, Harold, Ranyelle, Robin, Lalith, Rajat, Mr DeBoer and all the other great individuals that I have met on this journey.

Table of Contents

List of Figures

List of Schemes

List of Abbreviations

AcOH	acetic acid
BODIPY	boron dipyrromethene
d	doublet
DMF	*N*,*N*-dimethyl formamide
DMSO	dimethyl sulfoxide
DPA	dipicolyl amine
eT	electron transfer
EtOAc	ethyl acetate
EtOH	ethyl alcohol
FRET	Fluorescence Resonance Energy Transfer
h	hour
HMTA	Hexamethylenetetraamine
HOMO	highest occupied molecular orbital
ICT	internal charge transfer
LUMO	lowest unoccupied molecular orbital
m	multiplet
min	minute
MLCT	metal to ligand charge transfer
PeT	photoinduced electron transfer

ROS	reactive oxygen species
s	singlet
t	triplet
THF	tetrahydrofuran
TLC	thin layer chromatography
TPTN	*N,N,N′N′*(2-pyridylmethyl)-propylenediamine
UV-vis	ultraviolet visible

1 Introduction

1.1 Iron and Biology

Iron is the most abundant transition metal in the body and performs a diverse array of biological functions.[1] Living organisms, whether bacteria or mammals, require iron for many important biological processes such as respiration, reproduction and mammalian cellular growth. The functional diversity of iron in biological processes results primarily from its existence in two stable oxidation states, II and III. Healthy levels of the metal are maintained by homeostasis which ensures that the redox chelatable species does not exceed the normal binding capacity of the organism. Increase in brain iron concentration which accompanies aging, along with disruption in homeostasis can create a severe imbalance in the amount of labile iron. Ferrous iron in particular is known to react with hydrogen peroxide (H_2O_2) to produce hydroxide and more importantly hydroxyl free radicals ($^{\bullet}OH$) via the Fenton reaction.[2] This reactive oxygen species (ROS) has been suspected to be a key player in the pathogenesis of neurodegenerative diseases such as Alzheimer's and Parkinson's.[3-5] However, the definitive role of iron in these diseases continues to elude investigators and makes studying intracellular concentrations of the metal challenging.

1.2 Fluorescence Turn-On Probes

The success achieved by earlier small molecule fluorescence turn-on sensors in Ca(II)[6] and Zn(II)[7] intracellular detection has led to the extensive exploration of new candidates for other metals. This method of detection is largely attractive due to the high sensitivity afforded by fluorescence. Small molecule fluorescence turn-on sensors usually consist of an emissive reporter (fluorophore) that is covalently attached to a metal binding motif, commonly referred to as a receptor. A large number of fluorophore-receptor systems exist and most of these have been developed for Zn(II) sensing studies. On the other hand, similar probes for transition metals ions such as Fe(III), Fe(II) and Cu(II) remain scarce because they provide additional non-radiative pathways for excited fluorophores.

Emission enhancement of a reporter in the presence of a metal ion is achieved through a process known as signal transduction. To date a number of these mechanisms have been exploited to create sensors for metals and other analytes. The list includes photoinduced electron transfer (PeT),[8] internal charge transfer (ICT),[9] fluorescence resonance energy transfer (FRET),[10] and chemical transformation of a tethered receptor. Only examples utilizing PeT and the latter signal transduction mechanism will be discussed in this chapter.

1.3 Principles of PeT

PeT has been the most widely used signal transduction mechanism and only requires modest separation between fluorophore (acceptor) and receptor (donor). Many of these systems contain phenylene[11] or methylene[12] moieties called spacers that connect the donor and acceptor fragments. The relative orbital energies of both donor and acceptor largely influence the thermodynamics of the electron transfer process (Fig. 1.1). Efficient electron transfer which non-radiatively deactivates the excited states of fluorophores, occurs as long as the energy of the donor's HOMO is situated between the HOMO-LUMO gap on the acceptor. Metal binding events can reduce the donor's oxidation potential thus lowering its HOMO; electron transfer becomes inefficient as a result. Restoration of the fluorophore's emission usually accompanies this process. This fluorescence transduction mechanism allows for great sensitivity and involves design elements that are fairly simple compared to the others. In addition PeT can be potentially achieved by a wide array of fluorophore-receptor systems.

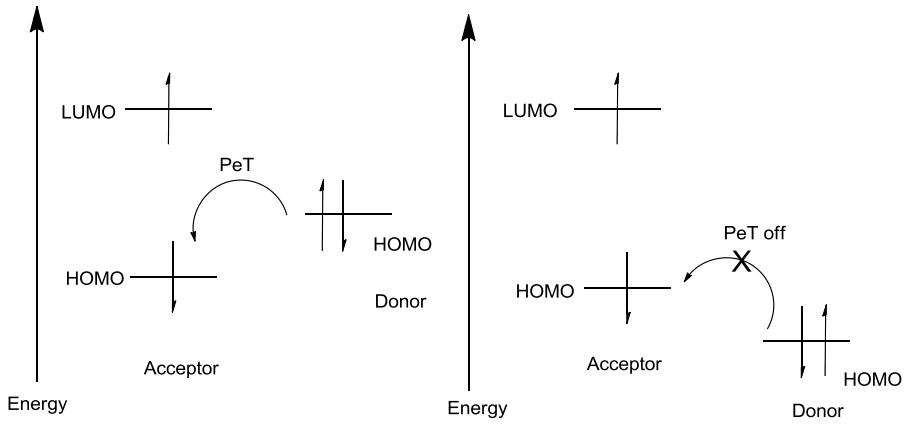

Figure 1.1 Frontier molecular orbital diagram of PeT process.

1.4 Examples of PeT-Based Sensors

Many zinc sensors are Pet-based systems and quite a few feature fluorescein platforms.[13-16] ZnPyr is one example. This probe contains a pair of dipicoly amine (DPA) receptors which in the unbound form reduced the emission of BODIPY fluorophore[8] (Fig.1.2). The interaction of ZnPyr with nanomolar concentrations of Zn(II) ions produced a 6-fold enhancement in emission with great selectivity. More importantly, Zn(II) ions in the hippocampus of mice could be detected using this probe.

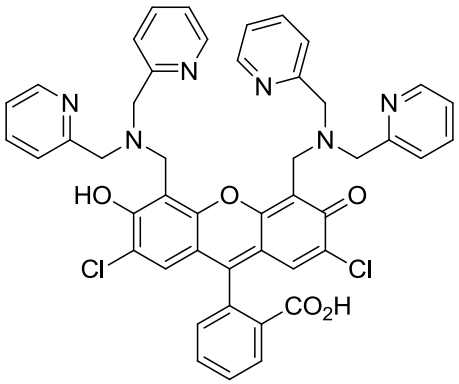

1

Figure 1.2 Structure of ZnPyr.

Aminonapthalimide derivatives can be fairly easily manipulated synthetically and as such are quite attractive systems for use in fluorescence sensing applications. Additionally, many naphthalimide-receptor dyads possess PeT functionality. Installing an aniline-DPA moiety at the imide side of the molecule produced **2**, which detected Zn(II) ions in cultured HeLa cells.[17] In the absence of the metal, **2** was weakly emissive owing to PeT from the DPA-based receptor to the naphthalimide fluorophore. The probe bound zinc tighly (K_d = 0.62 nM) and this restored the fluorescence with high quantum yield. Unlike fluorescein-based systems such as ZnPyr and the like, **2** is scarcely affected by pH.

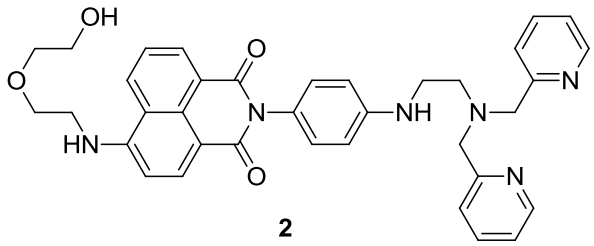

2

Figure 1.3 Structure of naphthalimide-based sensor.

1.4.1 PeT-Based Sensors for Fe(III)

The use of PeT in Fe(III) ion sensing is far less widespread than in the case of Zn(II) and only a handful of sensors have been reported to date. Coupling a crown ether receptor with an anthracene fluorophore produced **3** which displayed weak emission in its unbound form.[18] Titration with Fe(III) ions resulted in a significant emission enhancement with good sensitivity. In addition, **3** demonstrated the capability to detect this metal ion in the presence of others such as Mn(II), Pb(II), Co(II), Hg(II), Ni(II) and Cu(II). The probe also possessed the ability to work in conditions that are analogous to physiological environment, an important prerequisite for use in biological applications.

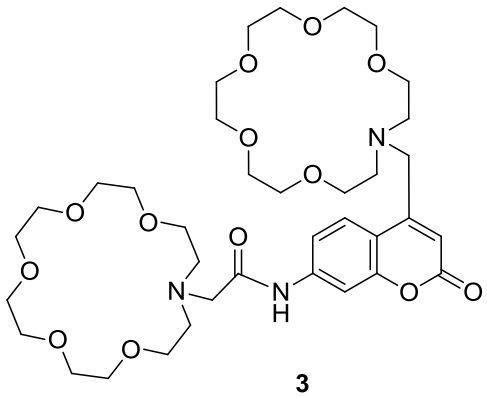

3

Figure 1.4 Structure of **3**.

Qian and co workers explored the use of a 4-amino-1,8–dicyanonaphthalene (ADCN) platform in metal ion sensing.[19] Electron transfer in ADCN is facilitated by the electron donating and withdrawing substituents on the molecule. In a manner similar to 1,8-aminonaphthalimide derivatives, attachment of a receptor at the donor side of the

molecule leads to efficient PeT. Compound **4** displayed weaker emission in polar solvents compared to non-polar ones. This is an intrinsic property of PeT systems. Coordination of Fe(III) and Cr(III) ions to the diamine receptor suppressed PeT and a 26-fold fluorescence enhancement was obtained in ethanol. The probe also proved to be pH sensitive owing to the presence of the triethylamine receptor, and thus can also be used to detect protons.

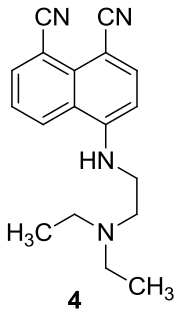

4

Figure 1.5 Structure of **4**.

High quantum yields and the ability to emit in many solvent systems render anthracene fluorophores to be highly coveted for use in many sensing applications. In many of these the receptor communicates with the fluorophore through PeT. Sensor **5** (Fig. 1.5) is such an example that was used to detect Fe(III) ions.[20] The apo form was weakly emissive due to efficient electron transfer from the tertiary amine tridentate receptor to the anthracene moiety. The absorption spectra of **5** in CH_3CN/H_2O consists primarily of a broad band (345-395 nm) that corresponds to the π-π^* transition of anthracene. Exciting **5** at 368 nm in the presence of Fe(III) produced a greater than 40-fold emission enhancement with great selectivity.

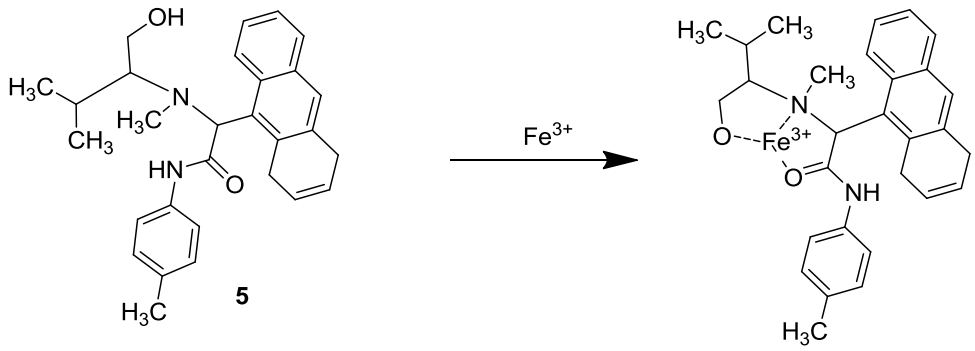

Figure 1.6 Fe(III) sensing by **5**.

1.5 Sensors Utilizing a Chemical Transformation of a Tethered Receptor

There is an emerging class of turn-on sensors whose fluorescence transduction mechanism is based on metal-induced chemical transformation of a tethered receptor. Many of these have been created for redox-active metals such as Cu(II) and Fe(II). Though such probes are usually irreversible, they are chemodosimeters, and hold the advantage of being inert to quenching by open shell transition metal ions. This is possible because the metal ion only facilitates a chemical reaction and its otherwise interaction with the fluorophore is minimized.

1.5.1 Fluorescence Probes for Cu(II)

A coumarin derivative capable of undergoing a Cu(II)-catalyzed hydrolysis of a hydrazone unit was synthesized by Kim and coworkers.[21] Sensor **6** was weakly fluorescent and coordinated to Cu(II) with micromolar binding constant. In the presence of H_2O, hydrolysis cleaved the imine bond (Fig 1.6) releasing the highly emissive coumarin derivative. Using this strategy Cu(II) could be detected selectively in very low concentrations since catalytic quantities of the metal induced significant changes in the emission intensity of **6**. Some reaction based systems suffer from slow response times; however, this sensor reportedly underwent complete transformation in approximately 8 min.

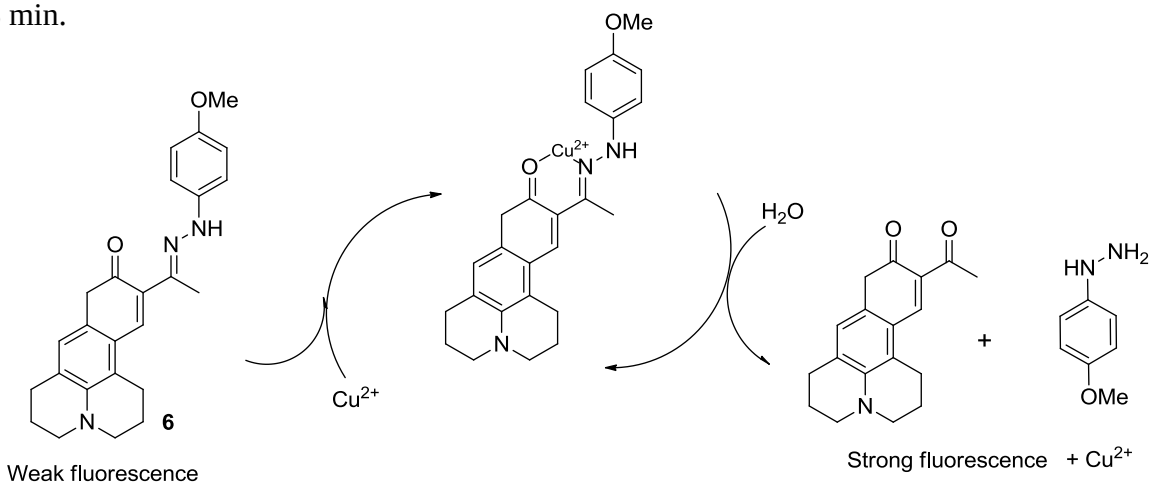

Figure 1.7 Mode of action of Cu(II) sensor.

A non-fluorescing coumarin **7** derivative was synthesized and the underlying mechanism governing Cu(II) detection was investigated.[22] Sensor **7** possessed a relatively high extinction coefficient and unlike **6** demonstrated its ability to operate in aqueous conditions. When titrated with up to 10 μM of Cu(II), **7** recorded a 50-fold emission enhancement. Titrations also suggested that a 2:1 ligand to metal complex was formed. Investigating the fluorescence transduction mechanism revealed that **7** first underwent coordination followed by hydrolysis of the lactone moiety (Fig. 1.7). In addition, the selectivity was excellent as other metal scarcely interfered with the sensor's ability to detect Cu(II).

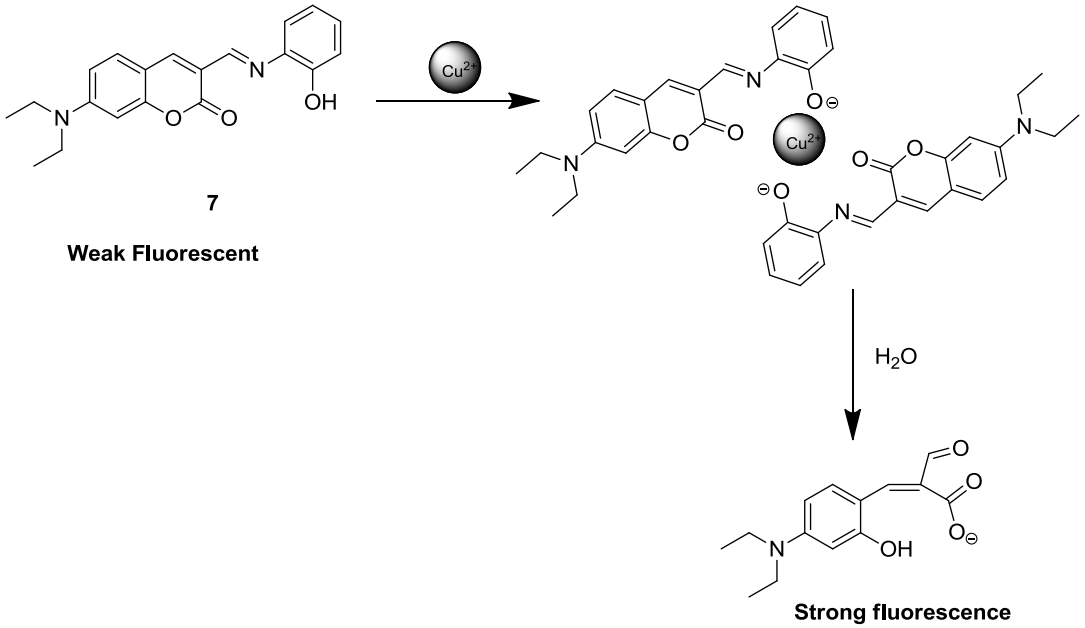

Figure 1.8 Fluorescence transduction mechanism of **7**.

Qi and coworkers demonstrated that it is possible to construct irreversible fluorescence turn-on sensors for metal ions using borondipyromethene (BODIPY) derivatives.[23] Compound **8** contained diacetate receptors (Fig. 1.8) that were tethered to the BODIPY scaffold. Metal recognition was achieved by hydrolysis of the ester which produced the highly fluorescent alcohol derivative. NMR evidence illustrated that Cu(II) remained attached to the final product indicating that the reaction pathway maybe non-catalytic. Since BODIPY was used as the reporting unit, the observed quantum yield of the terminal species was large (Φ =0.85) and as a result **8** was very sensitive to a wide concentration range of the metal ion.

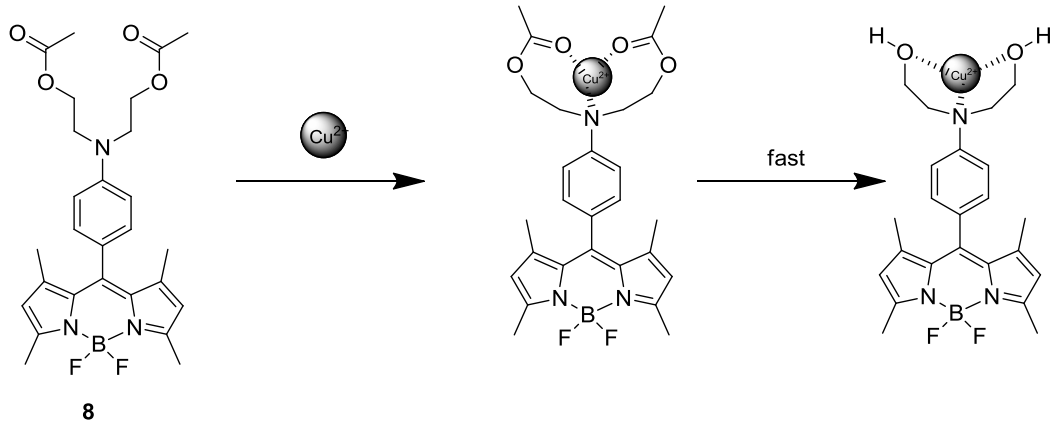

8

Figure 1.9 Detection of Cu(II) by BODIPY-based fluorescence probe.

1.5.2 Fluorescence Probes for Fe(III)

A small number of probes for Fe(III) ions have been designed using metal induced ring opening reactions. Rhodamine spirolactam substrates owing to the ease at which different units can be attached to their amide nitrogens are particularly attractive in these applications. In deed this strategy is very straight forward as the vast majority of the rhodamine derivatives in their spirolactam form are virtually non fluorescent. The addition of Fe(III) (1-450 μM) to **9** in CH_3CN-H_2O hydrolyzed the spirolactam to give the strongly fluorescent rhodamine imidate tautomer and 4–nitrosalycylaldehyde[24] (Fig. 1.9). The sensor was remarkably selective and showed capabilities to detect Fe(III) ions in live cells.

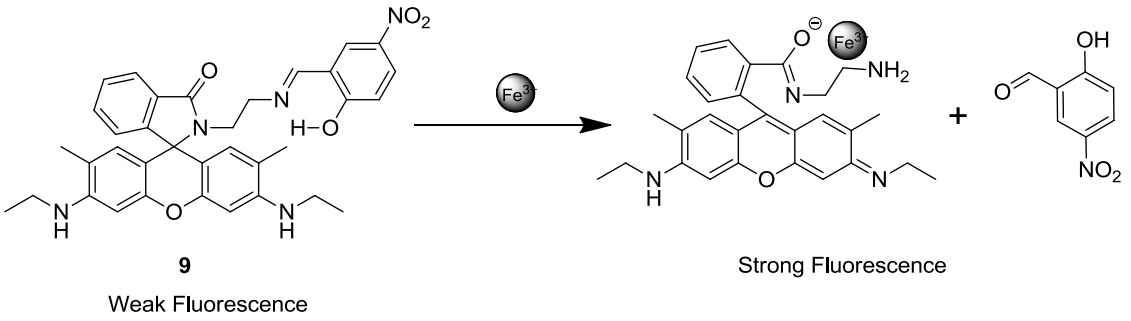

Figure 1.10 Iron-sensing mechanism using chemodosimeter **9**.

Reversible fluorescence probes can also be synthesized using rhodamine spirolactam derivatives. The ring opened imidate dyad of **10** coordinated with moderate binding constants to Fe(III) resulting in a 20–fold fluorescence enhancement in ethanol and aqueous media.[25] Treating **10** with excess EDTA removed the metal while the initial emission intensity was restored. Since profound changes in the absorption spectra accompanied metal binding **10** also functioned as a colorimetric probe for Fe(III).

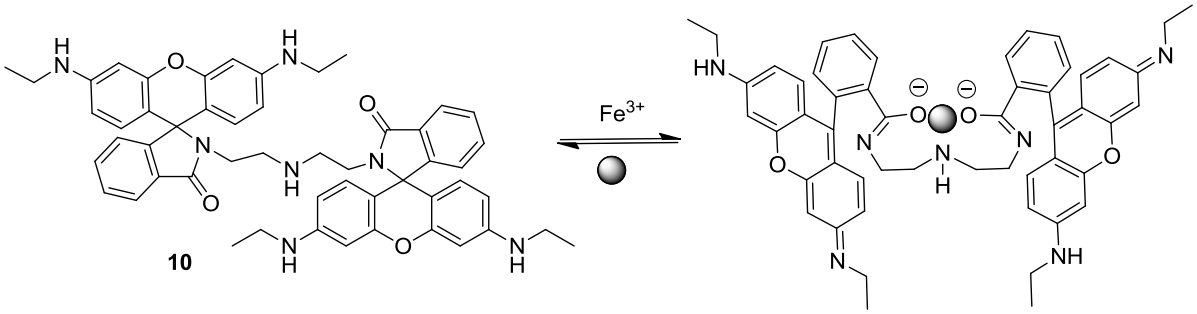

Figure 1.11 Structure and mechanism of action of reversible chemosensor **10**.

Lim and coworkers prepared a squarate-coumarin dyad, **11**, as a chemosensor for Fe(III).[26] A dual signal transduction mechanism was responsible for the observed emission enhancement in the presence of the metal ion. Weak fluorescence observed in the apo form of **11** was due to PeT quenching of the fluorophore. Addition of Fe(III) to the sensor in organic and aqueous solvents resulted in coordination to the squarate-hydroxamate moiety as evidenced by the existence of a transient charger

transfer band in the region 550-600 nm. Imine formation and subsequent hydrolysis proceeded metal interaction, releasing the free courmain fluorophore which was highly emissive. By using this method, **11** was also capable of selective recognition of the metal.

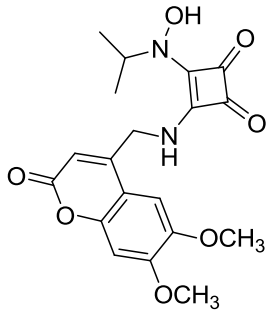

11

Figure 1.12 Chemical structure of squarate-hydroxamate sensor **11**.

1.6 Summary

Research in metal ion sensing is continually expanding to meet the demands for fluorescence probes in biological assays. Transition metals present the greatest challenge because of their intrinsic quenching behavior and several strategies have been explored to circumvent this issue, a few of which were discussed. Chemosensors that operate on the basis of metal induced redox reactions appear to be promising solutions to circumvent the quenching problem.

References

1. Aroun, A.; Zhong, J. L.; Tyrrell, R. M.; Pourzand, C., *Photochem. Photobiol. Sci.* **2012**, *11*, 118-134.

2. Haber, F.; Weiss, J., *Proc. R. Soc. London, Ser. A.* **1935**, *147*, 332-351.

3. Dexter, D. T., *Lancet* **1987**, *341*, 1219-1220.

4. Connor, J. R.; Snyder, B. S.; Beard, J. L.; Fine, R. E.; Mufson, E. J., *J. Neurosci. Res.* **1992**, *31*, 327-335.

5. Riederer, P., *J. Neurochem.* **1989**, *52*, 515-520.

6. Grynkiewicz, G.; Poenie, M.; Tsien, R. Y., *J. Biol. Chem.* **1985**, *260*, 3440-3450.

7. Frederickson, C. J.; Kasarskis, E. J.; Ringo, D.; Frederickson, R. E., *J. Neurosci.* **1987**, *20*, 91-103.

8. Burdette, S. C.; Walkup, G. K.; Springer, B.; Tsien, R. Y.; Lippard, S. J., *J. Am. Chem. Soc.* **2001**, *123*, 7831-7841.

9. Kollmannsberger, M.; Rurack, K.; Resch-Genger, U.; Daub, J., *J. Phys. Chem. A* **1998**, *102*, 10211-10220.

10. Jisha, V. S.; Thomas, A. J.; Ramaiah, D., *J. Org. Chem.* **2009**, *74*, 6667-6673.

11. Sunahara, H.; Urano, Y.; Kojima, H.; Nagano, T., *J. Am. Chem. Soc.* **2007**, *129*, 5597-5604.

12. Zeng, L.; Miller, E. W.; Prale, A.; Isacoff, E. Y.; Chang, C. J., *J. Am. Chem. Soc.* **2006**, *128*, 10-11.

13. Komatsu, K.; Kikuchi, K.; Kojima, H.; Urano, Y.; Nagano, T., *J. Am. Chem. Soc.* **2005**, *127*, 10197-10204.

14. Mikata, Y.; Wakamatsu, M.; Yano, S., *Dalton Trans.* **2005**, 545-550.

15. Nolan, E. M.; Lippard, S. J., *Acc. Chem. Res.* **2009**, *42*, 193-203.

16. Nolan, E. M.; Lippard, S. J., *Inorg. Chem.* **2004**, *43*, 8310-8317.

17. Wang, J.; Xiao, Y.; Zhang, Z.; Qian, X.; Yang, Y.; Xu, Q., *J. Mater. Chem.* **2005**, *2005*, 2836-2839.

18. Hua, J.; Wang, Y.-G., *Chem. Lett.* **2005**, 98-99.

19. Qian, X.; Xiao, Y., *Tetrahedron Lett.* **2002**, *43*, 2991-2994.

20. Sung, K.; Fu, H.; Hong, S., *J. Fluoresc.***2007**, *17*, 383-389.

21. Kim, M. H.; Jang, H. H.; Yi, S.; Chang, S.; Han, M. S., *Chem. Commun.* **2009**, 4838-4840.

22. Li, N.; Xiang, Y.; Tong, A., *Chem. Commun.* **2010**, *46*, 3363-3365.

23. Qi, X.; Jun, E. J.; Xu, L.; Kim, S.; Hong, J. S. J.; Yoon, Y. J.; Yoon, J., *J. Org. Chem.* **2006**, *71*, 2881-2884.

24. Lee, M. H.; Giap, T. V.; Kim, S. H.; Lee, Y. H.; Kang, C.; Kim, J. S., *Chem. Commun.* **2010**, *46*, 1407-1409.

25. Xiang, Y.; Tong, A., *Org. Lett.* **2006**, *8*, 1549-1552.

26. Lim, N. C.; Pavlova, S. V.; Brückner, C., *Inorg. Chem.* **2009**, *48*, 1173-1182.

2 FerriNaphth: A New Fluorescence Turn-on Probe for Fe^{3+}

2.1 Introduction

To address the need for fluorescence turn-on probes for Fe^{III}, the Burdette research group recently reported on the design and synthesis of a sensor for redox metal active metal ions.[1] In FerriBRIGHT, Fe^{III} and Cu^{II} oxidize a catechol appended to a BODIPY fluorophore into a quinone. The oxidation of the catechol interrupts photoinduced electron transfer (PeT) quenching of the fluorophore, which enhances the intensity of the probe's emission. In addition to this system, a reversible quinone/hydroquinone switch was used to construct a redox probe, which further demonstrates the ability to use the redox behavior of a tethered substrate to elicit a fluorescence response.[2]

The design element consists of a 1,4-quinone coupled to a BODIPY fluorophore via a phenylene spacer. The BODIPY-quinone dyad fluoresces weakly owing to PeT from the quinone moiety to the fluorophore. After exposure to a reducing agent, however, fluorescence increases because formation of the corresponding hydroquinone interrupts the PeT process. Additional fluorescent probes for biological oxidants have been reported that use similar BODIPY-quinone systems.[3, 4]

Sensors that emit at a different wavelength in the apo and bound forms possess advantages in biological imaging applications. Ratiometric sensors often involve internal charge transfer (ICT) to induce wavelength shifts. Several naphthalimide derived sensors for Cu^{II} take advantage of ICT to shift absorption and emission wavelengths,[5-8] suggesting that dyads comprised of these fluorophores and

metal-binding ligands are good candidates for fluorescent probes. We hypothesized that oxidizing a catechol ligand conjugated to a naphthalimide fluorophore would result in an ICT state that would shift the absorption and emission wavelengths sufficiently to efficiently detect Fe^{III}. Naphthalimide fluorophores are prototypical donor-acceptor systems, where conjugating an electron pair donor with one of the imide carbonyls leads to the maximum fluorescence output.[9] We reasoned that an aniline nitrogen linker would be the best candidate to couple the naphthalimide with the catechol because it would be conjugated to both the fluorophore and the metal receptor (Fig. 2.1).

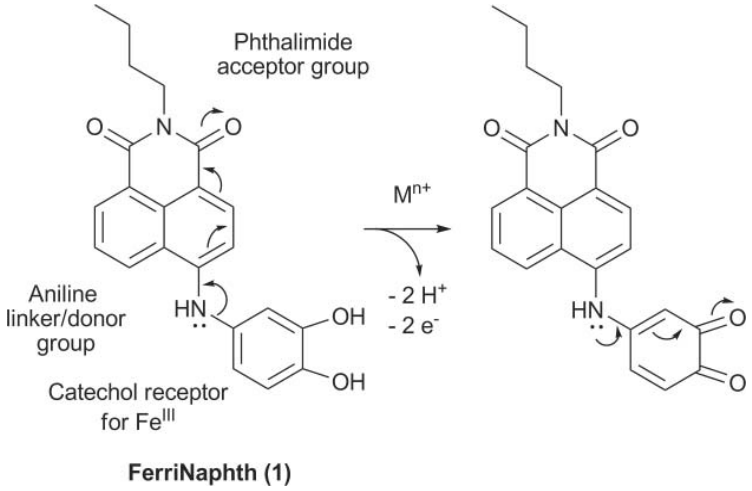

Figure 2.1 Design and signaling mechanism of FerriNaphth. In the absence of metal ions, the lone pair on the aniline nitrogen participates in a donor-acceptor resonance interaction with the phthalimide carbonyl group. After oxidation with Fe^{III}, the aniline also can engage in a resonace interaction with the quinonoe carbonyl, which would lead to different absorption and emission characteristics by an ICT.

2.2 Results and Discussion

The desired fluorescent probe was prepared using Pd-catalyzed aryl amination between 4-bromo-*N*-butyl-1,8-naphthalimide (**2**)[10] and 5-aminospiro(1,2-benzodioxole-2,1′-cyclohexane) (**3**)[11] that provided the precursor ligand in 58 % yield after purification by column chromatography (Scheme 2.1). Removal of the cyclohexylidene ketal with concentrated HCl provided FerriNaphth.

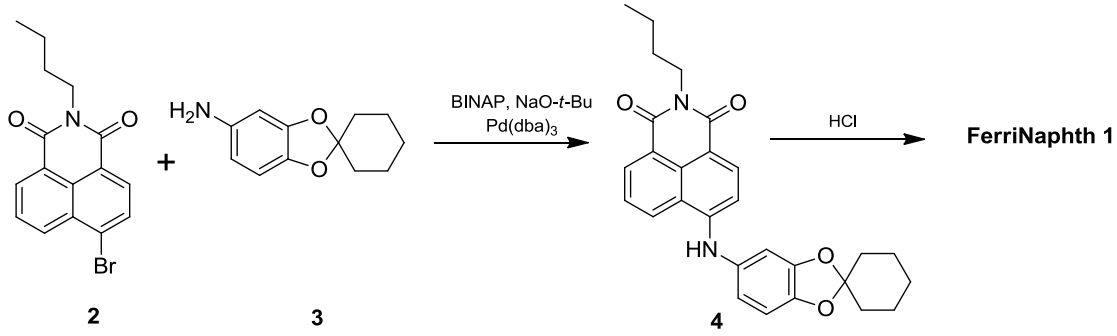

Scheme 2.1 Synthesis of FerriNaphth.

The name FerriNaphth is derived from the fluorophore (naphthalimide) and the target analyte (ferric ion). FerriNaphth is a red crystalline solid that is soluble in organic solvents, but only sparingly soluble in aqueous solution. When dissolved in anhydrous acetonitrile, FerriNapth absorbs with a λ_{max} at 441 nm (ε = 16200 $cm^{-1}M^{-1}$) and displays weak emission with a λ_{max} at 520 nm (Φ = 0.001). Upon exposure of FerriNaphth to $Fe(NO_3)_3$ the absorption peak at 441 nm degrades over a period of 3 min, with the concomitant formation of a new peak at 368 nm (Fig. 2.2, top). An increase in the emission intensity centered at 520 nm is observed after the addition of H_2O when excited at 400 nm (Fig. 2.2, bottom); however, no significant changes in

emission behavior are observed under anhydrous conditions. Similar changes are observed in the absorption spectra when CH_3OH was used as a solvent; however, the changes in emission are less pronounced. Using the nitrate salt eliminates bands from $FeCl_3$ and $Fe(ClO_4)_3$ that overlap the absorption peaks of FerriNaphth, but has no significant impact on the fluorescence response. Absorption bands blue-shift in typical ICT-based naphthalimide sensors, but emission wavelengths do not red shift.[13] Since the changes in the absorption spectra contradicted predicted ICT behavior, the product of iron oxidation was investigated. Analysis of solutions containing the probe and Fe^{III} by TLC revealed the presence of a fluorescent compound and a bright red species that decomposed upon solvent removal. The fluorescent compound was isolated and identified as *N* –*n*butyl-4-aminonaphthalimide (**7**).[9, 14] The presence of **7** suggests that instead of an ICT system, the fluorescence signal transduction mechanism of FerriNaphth involves metal-promoted oxidation, followed by a second chemical transformation.

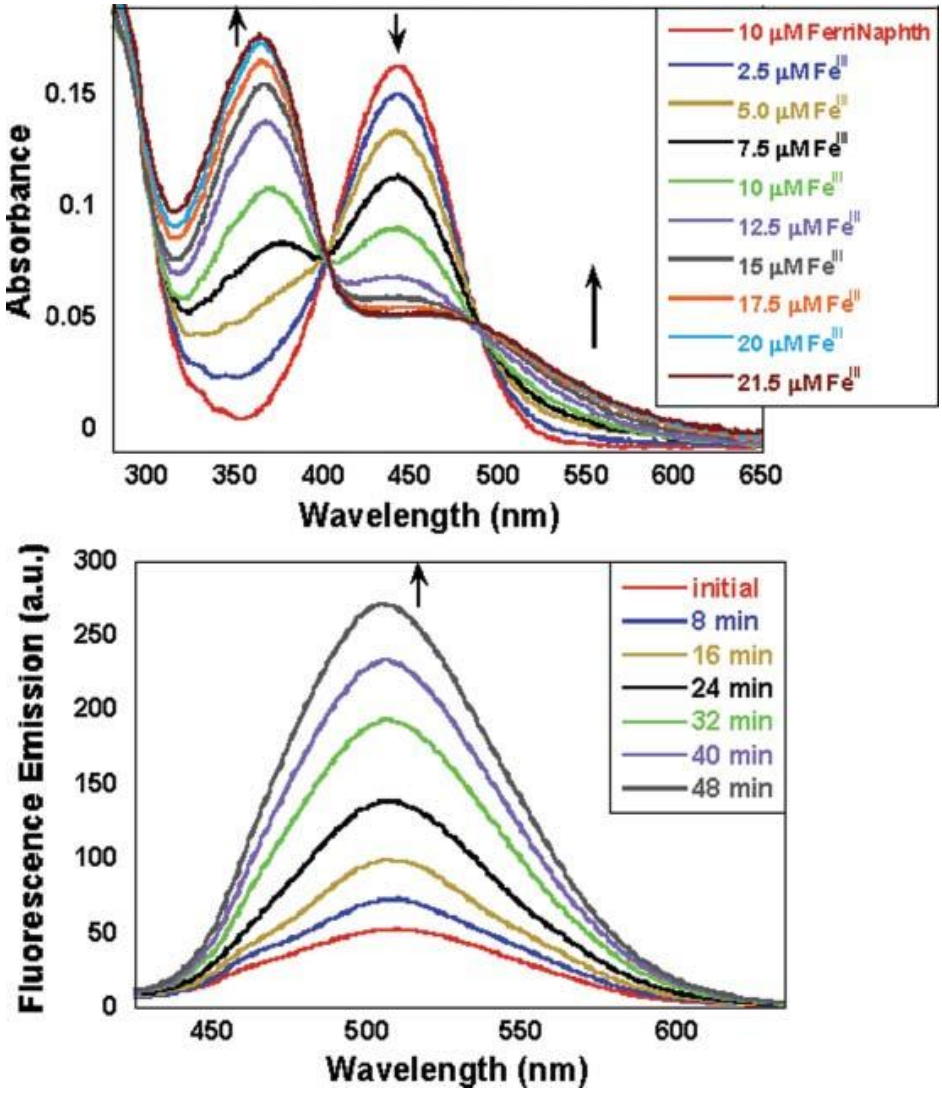

Figure 2.2 Oxidation of 10 μM FerriNaphth in CH_3CN with incremental additions of $Fe(NO_3)_3$. Absorbance (top) measurements were recorded after no additional changes were observed after each addition. Emission spectra (bottom) were recorded over a period of 48 min after the addition of 2 equivalents of $Fe(NO_3)_3$ and 1% H_2O by volume. Excitation was provided at 400 nm.

Aminooxyquinones like **5** are tautomeric red compounds,[15] and investigations revealed that the addition of water and 10 mol% pyridyl *p*-toluenesulfonic acid accelerate the disappearance of the red species and increase the intensity of emission from **7**. These observations suggest that oxidized FerriNaphth, which can exist in both a quinone (**5**) and an imine-one tautomer (**6**), subsequently undergoes imine hydrolysis to provide the fluorescent naphthalimide **7** (Scheme 2.2). In addition to this mechanistic evidence, a charge transfer band at 362 nm corresponding to the $[Fe(ferrozine)_3]^{4-}$ complex forms when FerriNaphth is oxidized by Fe^{III} in the presence of ferrozine, a common Fe^{II} indicator (Fig. 2.6). The catechol to quinone transformation requires a 2 electron oxidation which corresponds to approximately 2 equivalents of ferric iron reacting with every equivalent of FerriNaphth in solution.

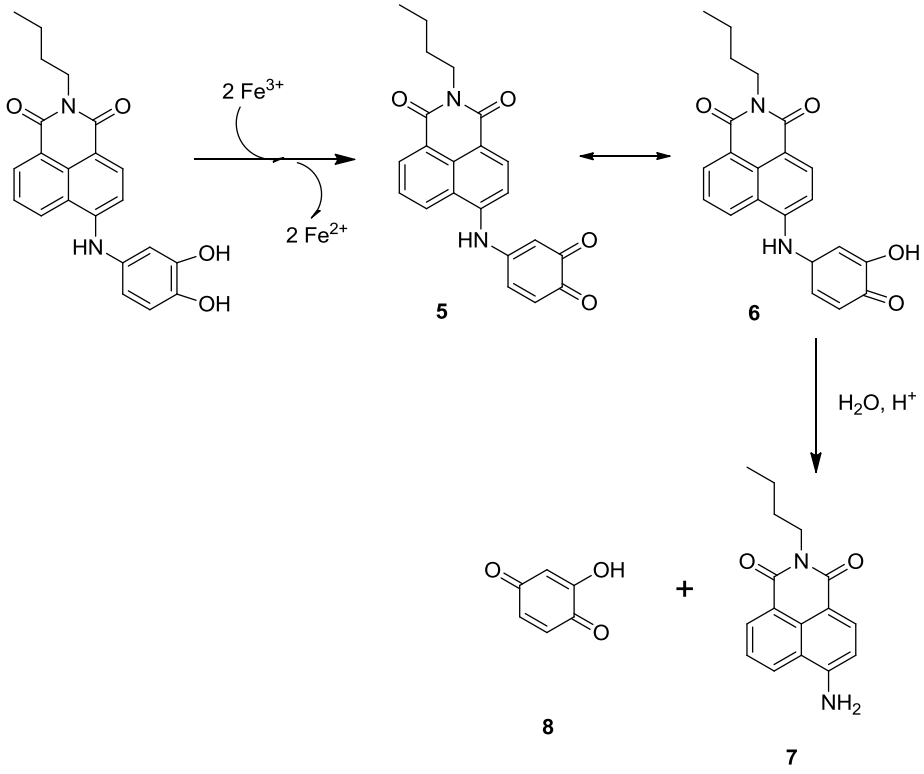

Scheme 2.2 Fluorescence transduction mechanism of FerriNaphth.

Relatively few chemodosimeters have been designed where a turn-on fluorescence signal results from the hydrolysis of the weakly fluorescent parent molecule.[16-20] Typically these probes exploit the Lewis acidity of a metal ion to promote the liberation of a fluorophore that is quenched by the reactive bonding interactions. In a probe that selectively responds to Fe^{III}, Schiff bases from the chelating ligand hydrolyze to release a highly fluorescent coumarin fluorophore. While other chemodosimeters for Fe^{III} based on oxidation chemistry and fluorophore isomerization have been reported there has been only one report of a system utilizing both oxidation and hydrolysis to achieve an emission enhancement in the presence of a redox active transition metal.[21] In the squaride hydroxamate system, however multiple products from the redox process were observed and only a few that were responsible for the emission enhancement were characterized successfully.

The emission intensity of **7** is polarity dependent, and has a quantum yield of 0.74 in CH_3CN.[9] Repeating the fluorescence assay in nonpolar solvents like THF and CH_2Cl_2 with 1% H_2O provides a more intense fluorescence signal. Experiments using protic solvents like H_2O and CH_3OH only result in weak emission responses. Completely drying alcoholic solvents is difficult, which explains why emission changes are observed in CH_3OH without the addition of exogenous water and why the absorption spectra of oxidized FerriNaphth erodes slowly over time. Additional attempts to enhance the rate of fluorescence response from FerriNaphth were unsuccessful. While the initial oxidation step is complete within minutes with stoichiometric Fe^{III}, hydrolysis remains very slow even with the addition of catalytic water and acid. Evaluation of the emission intensity of FerriNaphth over time with Fe^{III} in the presence of water, CH_3COOH, H_3PO_4 and HNO_3

showed varying rates in the emission increase, although hydrolysis requires a period of several hours and remains incomplete even after several days. The slow fluorescence response of FerriNaphth and the incompatibility of naphthalimide fluorescence properties to aqueous conditions limit the potential biological application of this probe, but represent a unique signal transduction mechanism that could be adapted for such purposes.

In order to confirm the fluorescence signaling mechanism of FerriNaphth, we sought to confirm the identity of the quinone/imine-one tautomeric intermediate. In thoroughly dried CH_3CN, the peak at 368 nm corresponding to oxidized FerriNaphth remains stable for extended periods of time; however only **7** can be isolated when the solvent is removed. The tautomeric species shows no appreciable fluorescence, which suggests the increase in emission intensity observed in the fluorescence studies can be attributed solely to **7.** Recently, a napthalimide-based Zn^{2+} sensor has been reported that fluoresces at different wavelengths in its two tautomeric forms.[22] Since the intermediate remains stable in solution, tandem mass spectrometric (MS/MS) analysis was performed (Fig. 2.3).

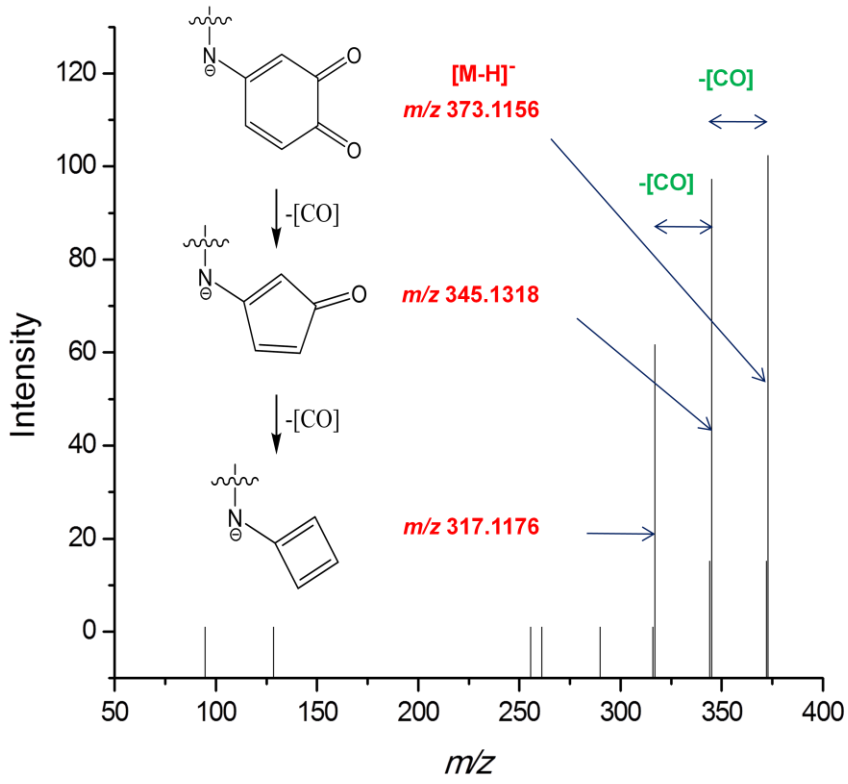

Figure 2.3 MS/MS analysis of oxidized FerriNaphth. The presence of quinoline anions as well as peaks corresponding to the loss of CO units verify the identity of the oxidation product.

In addition to detecting a parent ion corresponding to a molecular weight of 2 amu less than FerriNaphth, a fragmentation pattern consistent with the step-wise loss of two CO units was also observed. The combined experimental results suggest that catechol oxidation followed by hydrolysis of a tautomeric quinone/imineone correctly describes the mechanism of fluorescence enhancement. To determine the extent of FerriNaphth's ability to detect metal oxidants, the probe was exposed to a variety of

different oxidants at several different concentrations. $Cu(NO_3)_2$ oxidizes FerriNaphth (Fig. 2.4), and changes in the absorption spectra are similar to those measured in using Fe^{III} although Cu^{II} has a higher standard reduction potential that is ~ 0.6 V lower than Fe^{III}. Since the oxidation is relatively rapid, it is difficult to compare the rates of oxidation with the two metals with standard UV-Vis instrumentation. Stopped flow techniques could elucidate more detailed kinetic information and may provide a methodology to discriminate between the two metal ions by rate analysis.

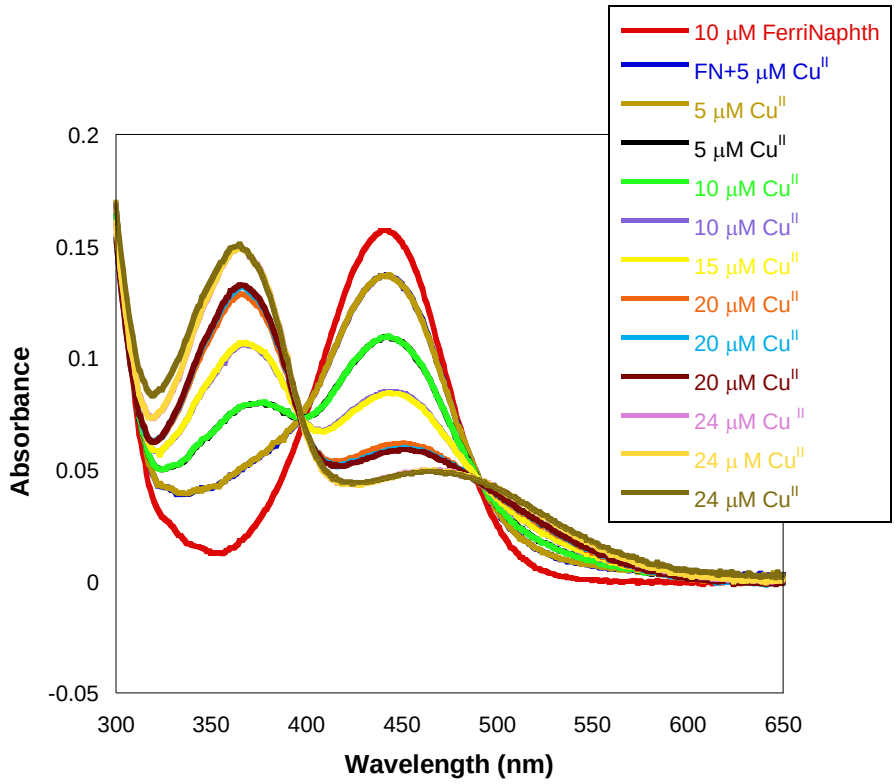

Figure 2.4 Oxidation of FerriNaphth by $Cu(NO_3)_3$.

In a manner analogous to Fe^{III}/Ferrozine assay, oxidation of FerriNaphth with Cu^{II} in the presence of Neocuproine, a common indicator for Cu^1, results in a strong

band at 480 nm that is indicative of $[Cu(neocuproine)]^{+}$ indicating approximately 2 equivalents of Cu^{II} are consumed in the oxidation (Fig. 2.5)

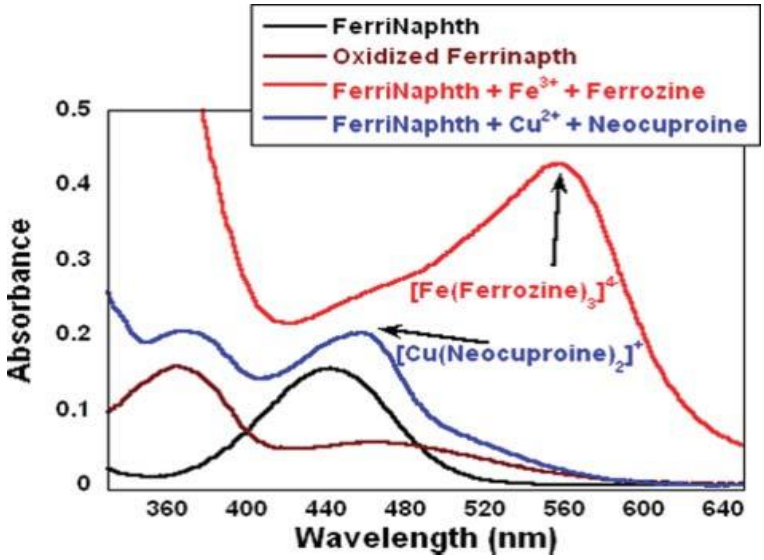

Figure 2.5 Absorbance spectra of 10 µM FerriNaphth (in CH_3CN) with Cu^{II}/Fe^{III} in the presence of Ferrozine/Neocuproine.

FerriNaphth does not oxidize in the presence of $AgNO_3$, which has a slightly more positive standard reduction potential than Fe^{III}, even at high concentrations of the metal ion. Ag^{1} does not coordinate strongly with catechol ligands like those in FerriNaphth, suggesting that coordination of metal ion to the ligand facilitates oxidation. This conclusion is supported further by the results of assays using $Fe(CN)_6^{3-}$ and $[Co(NH_3)_5Cl]Cl_2$ as oxidants. Exposure of FerriNaphth to 10 or more equivalents of coordinatively saturated $Fe(CN)_6^{3-}$ shows no evidence of oxidation. FerriNaphth slowly oxidizes in the presence of $[Co(NH_3)_5Cl]Cl_2$ but the reaction remains incomplete after

48 h (Fig. 2.6).

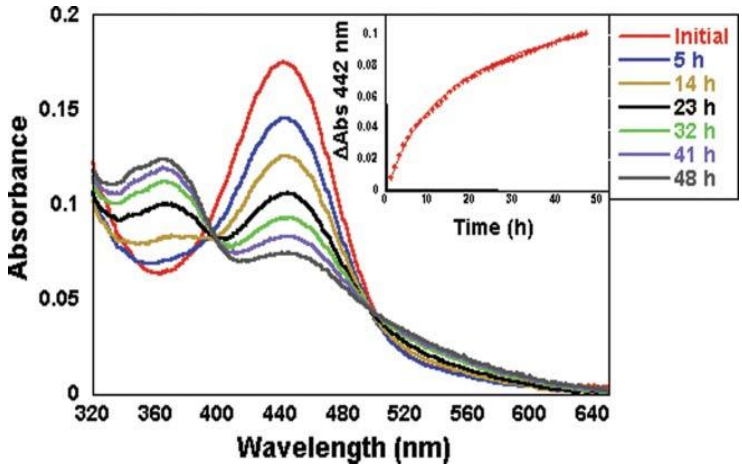

Figure 2.6 Oxidation of 10 μM with 6 equivalents of $Co[(NH)_5Cl]Cl_2$ in CH_3CN. The absorption spectra were automatically recorded every 48 h. Inset: changes in the absolute value of the absorbance at 442 nm as a function of time.

Even though Co^{III} is a strong oxidant, slow ligand exchange[23] with $Co[(NH)_5Cl]Cl_2$ results in decreased rates of oxidation. Unlike the other common oxidants screened, ceric ammonium nitrate causes decomposition of the probe into several unidentifiable products suggesting FerriNaphth is incompatible with especially strong oxidants.

Since the rapid oxidation of FerriNaphth precludes examination of coordination chemistry, the redox inert analog of Fe^{III}, Ga^{III}, was employed for additional studies. In addition to coordination chemistry, Ga^{III} allows the examination of ICT states produced by metal ion binding when FerriNaphth is not oxidized. Titration of FerriNaphth with up to 20 equivalents of $Ga(NO_3)_3$ results in a slight red shifting (~7 nm) and a decrease in

intensity of the absorption band centered at 441 nm and an increase in the absorption band at 360 nm. Ga^{III} titrations were carried out with the nitrate salt in MeOH because of limited solubility in CH_3CN; in addition, there are no readily available Ga^{III} salts that are compatible with the procedures used to assess FeriNaphth oxidation. When the FerriNaphth-Ga^{III} species is excited at 450 nm, a modest 2-fold increase in the emission intensity can be measured (Fig. 2.7). The spectroscopic changes suggest Ga^{III} binds to catechol generating an ICT state; however, the interaction does not appear to be very strong. At higher concentrations of $Ga(NO_3)_3$, evidence of FerriNaphth oxidization exists.

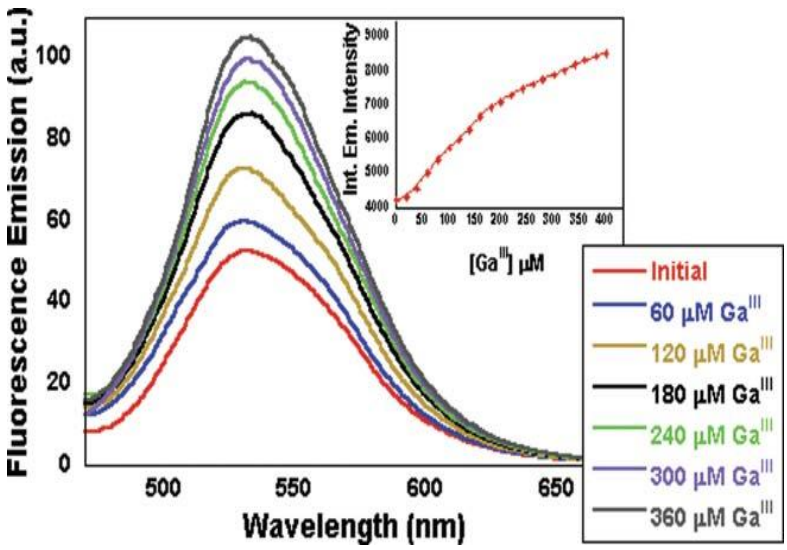

Figure 2.7 Titration of 10 µM FerriNaphth with $Ga(NO_3)_3$ in CH_3CN. Spectra were taken at 20 µM increments up to 360 µM of $Ga(NO_3)_3$, nitrate mediated oxidation of FerriNaphth starts to occur. Each spectrum was corrected for dilution by multiplying the measured absorption and integrated emission intensity by the inverse dilution factor. The emission intensity was integrated from 470 nm to 650 nm. Excitation was provided at 450 nm. Inset: changes in the integrated fluorescence emission with increasing concentrations of Ga^{III}.

Ga^{III} coordination to FerriNaphth lowers the pK_a of the coordinated phenols, which generates the conditions necessary for nitrate to act as an electron acceptor. Excess KNO_3 under acidic conditions also slowly oxidizes FerriNaphth. By adding additional acid to a solution containing FerriNaphth and 30 equivalents of $Ga(NO_3)_3$, the slow oxidation accelerates slightly. Fluorescence studies with Ga^{III} were carried out with 3 equivalents of Hunig's base to differentiate metal-based ICT states from ones resulting from oxidation. While some evidence of complexation between Ga^{III} and FerriNaphth was acquired, the persistence of oxidation reactions makes characterizing these weakly binding complexes difficult and ambiguous.

2.3 Conclusions

In summary we have prepared and characterized a new fluorescent chemodosimeter for metal based oxidants based on a tandem-hydrolysis reaction of a catechol linked naphthalimide-dyad. FerriNaphth has a weak emission that increases significantly upon conversion into *N* –^{n}butyl-1-4-aminonaphthalimide in the presence of Cu^{II} and Fe^{III}. Non-coordinating metal oxidants and redox inactive metal ions have only a minimal effect on the absorption and emission properties of FerriNaphth. The absorption changes are similar to some recently described Cu^{II} sensors that possess similar aniline components and are deprotonated by metal ion coordination,[5] but additional studies are needed to make meaningful comparisons. The signaling mechanism has been confirmed by isolation of the fluorescent species, detection of the reduced Fe^{II} in a fluorescence assay, and characterization of the oxidized intermediate by mass spectroscopy. Future efforts will involve designing a chemodosimeter with an ICT mechanism by stabilizing the linkage between catechol and fluorophore to inhibit hydrolysis.

Portions of this chapter were published as:

Jackson, R. K.; Shi, Y.; Yao, X.; Burdette, S. C., FerriNaphth: A Fluorescent Chemodosimeter for Redox Active Metal Ions. *Dalton Trans*., **2010**, *39*, 4155-4161

2.4 Experimental

General procedures. All materials listed below were of research grade or of spectrograde of highest purity available from TCI. Toluene and tetrahydrofuran (THF) were sparged with argon and dried by passage through a Seca Solvent Purification system. Chromatography and TLC were performed on silica (230-400 mesh) obtained from Silicycle. TLCs were developed with mixtures of EtOAC/hexanes or CH_2Cl_2 unless otherwise stated. 4-Bromo-*N*-butyl-1,8-napthalimide (**2**)[10] and 5-aminospiro(1,2-benzodioxole-2,1cyclohexane) (**3**)[11] were prepared according to literature procedures. ^1H and ^{13}C were recorded using a Bruker 400 MHz NMR instrument. Chemical shifts are reported in ppm relative to tetramethylsilane. IR spectra were recorded on a Nicolet 205 FT-IR instrument and samples were prepared as KBr pellets. High resolution mass spectra were recorded at the University of Connecticut mass spectrometry facility using a micromass Q-Tof-2^{TM} operating in positive mode

2.4.1 2-Butyl-6-spiro(1,3-benzodioxole-2-1′-cyclohexane-phenyl-amino)-benzo[de]isoquinoline-1,3-dione (4).

A schlenk tube was charged with 600 mg (1.18 mmol) of **2**, 408 mg (2.0 mmol) of **3**, 26 mg of BINAP (2.3 mol %), 18 mg $Pd(dba)_3$, 480 mg (5.0 mmol) of sodium tertiary butoxide and toluene (100 mL). The process of freeze–pump–thaw was repeated and the tube was back-filled with nitrogen, then sealed and heated to 90 °C while stirring for 48 h. The mixture was filtered through Celite, followed by repeated washing of the residue with dichloromethane. Solvent was removed by reduced pressure to yield an orange-brown solid. Flash chromatography on silica using ethyl acetate/hexanes (4: 1) yielded an orange solid (775 mg, 58%). TLC R_f = 0.25, 4/1 ethyl acetate/hexanes. ^1H NMR (400 Mhz, $CDCl_3$) δ

8.47 (d, J = 7.2, 1 H), 8.41 (d, J = 8.4, 1 H), 8.27 (d, J = 8.52, 1 H), 7.7 (t, J = 7.52, 1 H), 7.1 (d, J = 8.6, 1 H), 6.80-7.72 (m, 4 H), 4.20 (t, J = 6.92, 2 H), 1.99-1.96 (m, 4 H), 1.78-1.69 (m, 6 H), 1.49-1.41 (m, 2 H), 1.29-1.25 (m, 1 H), 1.01-0.96 (m, 3 H). ^{13}C NMR (100 MHz, $CDCl_3$) δ 164.8, 164.2, 184.8, 184.3, 145.9, 133.9, 132.8, 131.5, 130.1, 126.2, 125.4, 121.2, 117.10, 112.6, 108.8, 108.1, 106.1, 40.2, 35.4, 35.4, 34.9, 34.9, 30.5, 25.5, 24.7, 23.4, 20.6, 14.1. IR (KBr, cm^{-1}) 3349.2, 2935.9, 1684.8, 1640.9, 1581.7, 1535.4, 1429.5, 1390.4, 1361.0, 1344.6, 1240.7. HRMS (+ESI): Calcd. for M Na^+ 479.1947; Found, 479.1993.

2.4.2 2-Butyl-6-(3,4-dihydroxy-phenylamino)-benzo[de]isoquinoline-1,3-dione

(FerriNaphth 1). Concentrated hydrochloric acid (16 mL) was added to a stirred suspension of **5** (300 mg, 0.65 mmol) in absolute ethanol (25 mL). The mixture was refluxed for 90 min followed by the removal of half of the solvent by vacuum. Water was added to precipitate a red solid. This was filtered and washed (2 × 5 mL) with water. The solid was collected and chromatographed on silica using 100% dichloromethane to yield a red crystalline solid (185 mg, 75%). TLC R_f = 0.2, dichloromethane. ^{1}H NMR (400 MHz, DMSO) δ (s, 2 H), 8.97 (s, 1 H), 8.82 (d, J = 8.7 H, 1 H), 8.48 (d, J = 7.1 Hz, 1 H), 8.22 (d, J = 8.3 Hz, 1 H), 7.76 (t, J = 8.0 Hz, 1 H), 6.96 (d, J = 8.5 Hz, 1H), 6.84 (d, J = 8.2 Hz, 1 H), 6.78, (s, 1 H), 6.67 (d, J = 8.4 Hz,1 H), 4.04 (t, J = 7.5 Hz, 2 H), 1.63 (sextet, J = 6.8 Hz, 2 H), 1.34 (septuplet, J = 7.4, 2 H), 0.94 (t, J = 7.2, 3 H) ^{13}C NMR (400 MHz, DMSO) δ 164.4, 163.5, 150.4, 146.7, 143.9, 134.4, 131.7, 131.6, 130.3, 129.5, 125.4, 122.6, 121.3, 116.7, 116.4, 113.3, 109.9, 107.1 IR (KBr, cm^{-1}) 3390.1, 3290.8, 2956.6, 2925.2, 1685.5, 1674.5 1638.3, 1612.1, 1580.5, 1565.4, 1542.1, 1530.1,1520.6.

HRMS (+ESI): Calcd. for M Na^+ 399.1321; Found, 399.1352.

General methods. All solutions were prepared with spectrophotometric grade solvents FerriNaphth was dissolved in DMSO to make a 10 mM stock solution. A 3 mL aliquot of FerriNaphth stock was placed in a quartz cuvette and diluted with 3 mL of CH_3CN to provide a 10 mM solution for spectroscopy unless otherwise noted. Stock solutions (10 mM) of each metal ion were prepared in 3/2 EtOH/CH_3CN unless otherwise noted. Absorption spectra were recorded on a Cary 50 UV-visible spectrophotometer operated by a PC equipped with Pentium- IV processor. Spectra were taken at 25 °C in 1 cm path length cuvettes. Fluorescence spectra were recorded on a Hitachi F-400 spectrophotometer operated by a PC equipped with a Pentium-IV processor, running the FL solutions 2.0 software. A 150 W Xe lamp operating at 5 A provided excitation. Spectra were acquired in a quartz cuvette with a 1-cm path length. Slit widths are 5 nm for excitation and 10 nm for emission with a photomultiplier tube voltage of 700 V, unless stated otherwise.

UV-Vis experiments with $K_3Fe(CN)_6$, $AgNO_3$ and $[Co(NH)_5Cl]Cl_2$. For $K_3Fe(CN)_6$ and $AgNO_3$, the initial spectrum of a 10 μM solution of FerriNaphth was recorded which was followed by the addition of 2 equivalents of the metal complex. The spectra were monitored for changes over a period of 20 min. An additional 8 equivalents of metal complex was added to the cuvette and spectra were monitored for an additional 10 min. The experiment was repeated using 1.71 mM stock solution of $[Co(NH)_5Cl]Cl_2$ which was prepared in 2/1/1 MeOH/DMSO/H_2O. The initial spectrum of a 10 μM solution of FerriNaphth was recorded followed by the addition of a 6-fold excess of metal. Spectra were recorded every hour for 48 h.

UV-vis experiments with Ferrozine and Neocuproine. Commercially available ferrozine indicator was dissolved in 4/1 MeOH/H_2O to make 10 mM stock solutions. A 1 mM stock solution of $Fe(NO_3)_3$ was prepared in 9/1 CH_3CN/EtOH. Solutions were prepared by mixing 10 μM of FerriNaphth in CH_3CN with a 10-fold excess of both indicator and metal ion. The mixture was allowed to equilibrate for 0.5 h and the spectrum was recorded. Commercially available Neocuproine indicator was dissolved in CH_3CN to make a 10 mM solution, and analogous procedures to the Ferrozine assay were utilized for the Neocuproine experiment except a 20-fold excess of indicator was used.

Emission studies with Fe(NO3)3 . Spectra of 10 mM of FerriNaphth in CH_3CN was recorded before and after oxidation with $Fe(NO_3)_3$. After the addition of 30 mL of H_2O, an emission spectrum was recorded every 8 min for 48 min. The excitation wavelength was λ_{ex} = 400 nm. The excitation slit width was 5 nm and the emission slit width was 10 nm.

Emission studies with $Ga(NO_3)_3$. Stock solution of 10 mM $Ga(NO_3)_3$ was prepared in a 9/1 MeOH/DMSO. The initial emission spectrum of 10 mM solution of FerriNaphth in MeOH was recorded followed by the addition of metal in 20 mM increments. Spectra were recorded after each addition. The excitation wavelength was λ_{ex} = 450 nm. The excitation slit width was 5 nm and the emission 10 nm. The area under the emission spectra was integrated between 470–650 nm. The absorption spectra were recorded after the addition each 20 mM increment of metal.

Quantum yields. Quantum yields were calculated by measuring the integrated emission area of the corrected spectra and comparing that value to the area measured for Quinine in 0.5 M H_2SO_4 when excited at 365 nm (Φ_{fl} = 0.54).[12] The quantum yields

for FerriNaphth were calculated using eqn (1), where *F* represents the area under the emission spectra for the standard samples, *h* is the refractive index of the solvent and *Abs* is the absorbance at the excitation wavelength selected for the standard and samples. Emission spectra were integrated between 440–640 nm (λ_{ex} = 400 nm, 10^{-6} M/abs_{400} ~ 0.1).

$$\Phi_{fl}^{sample} = \Phi_{fl}^{standard}\left[\frac{F^{sample}}{F^{standard}}\right]\left[\frac{\eta^{sample}}{\eta^{standard}}\right]\left[\frac{Abs^{standard}}{Abs^{sample}}\right] \quad (1)$$

Mass spectroscopy. Tandem mass spectrometric (MS/MS) analysis was performed on a quadrupole-time-of flight tandem mas spectrometer (QTOFmicro, Waters, Milford, MA), equipped with an in-house modified electrospray (ESI) source. The compound was dissolved in CH_3CN and diluted with 10 mM ammonium bicarbonate in CH_3CN/H_2O (1:1, v/v). The sample solution was infused to a mass spectrometer with a flow rate of 50 µL min^{-1}. Key instrument parameters for the mass spectrometer, run under negative ion mode, were as follows: capillary voltage 2800 V, cone voltage (CV) 15 V, extraction voltage 2 V, collision energy (CE) offset 25 V. The MS/MS spectrum was obtained by selecting the negatively charged molecular ion ($[M - H]^-$, *m/z* 373.1) as precursor. The proposed fragmentation mechanism (loss of CO) was based on the accurate mass measurement.

References

1. Kennedy, D. P.; Kormos, C. M.; Burdette, S. C., *J. Am. Chem. Soc.* **2009**, *131*, 8578-8586.

2. Benniston, A. C.; Copley, G.; Elliot, K. J.; Harrington, R. W.; Clegg, W., *Eur. Org. Chem.* **2008**, 2705-2713.

3. Sun, Z. N.; Wang, H. L.; Liu, F. Q.; Chen, Y.; Tam, P. K. H.; Yang, D., *Org. Lett.* **2008**, *10*, 2171-2174.

4. Sun, Z. N.; Wang, H. L.; Liu, F. Q.; Chen, Y.; Tam, P. K. H.; Yang, D., *Org. Lett.* **2009**, *11*, 1887-1889.

5. Huang, J. H.; Xu, Y. F.; Qian, X. H. *Dalton Trans.* **2009**, 1761-1766.

6. Huang, J. H.; Xu, Y. F.; Qian, X. *Org. Biomol. Chem.* **2009**, *7*, 1299-1303.

7. Xu, Z. C.; Xiao, Y.; Qian, X. H.; Cui, J. N.; Cui, D. W., *Org. Lett.* **2005**, *7*, 889-892.

8. Xu, Z. C.; Qian, X. H.; Cui, J. N. *Org. Lett.* **2005**, *7*, 3029-3032.

9. Saha, S.; Samantha, A., *J. Phys. Chem. A* **2002**, *106*, 4763-4771.

10. Liu, B.; Tian, H. *Chem. Commun.* **2005**, 3156-3158.

11. Clark, R. L.; Pessolano, A. A.; Shen, T. -Y.; Jacobus, D. P.; Jones, H.; Lotti, V. J.; Flataker, M. L., *J. Med. Chem.* **1978**, *21*, 965-978.

12. Crosby, G. A.; Demas, J. N., *J. Phys. Chem.* **1971**, *75*, 991-1024.

13. Srikun, D.; Miller, E. W.; Dornaille, D. W.; Chang, C. J., *J. Am. Chem. Soc.* **2008**, *130*, 4596-4597.

14. Alexiou, M. S.; Tychopoulos, V.; Ghorbanian, S.; Tyman, T. H. P.; Brown, R. G.; Brittain, P. I., *J. Chem. Soc. , Perkin Trans.* **1990**, *2*, 837-842.

15. Liberato, D. J.; Byers, V. S.; Dennick, R. G.; Jr, N. C., *J. Med. Chem.* **1981**, *24*, 28-33.

16. Oshimmima, R.; Kitamura, M.; Morita, A.; Shiro, M.; Yamada, Y.; Ikekita, M.; Kimura, E.; Aoki, S., *Inorg. Chem.* **2010**, *49*, 888-889.

17. Lin, W. Y.; Yuan, L.; Feng, J. B.; Cao, W. X., *Org. Lett.* **2008**, 2689-2692.

18. Aoki, S.; Sakurama, K.; Oshima, R.; Matsuo, N.; Yamada, Y.; Takasawa, R.; Tanuma, S. I.; Talkeda, K.; Kimura, E., *Inorg. Chem.* **2008**, *47*, 2447-2454.

19. Qi, X.; Jun, E. J.; Xu, L.; Kim, S. J.; Hong, J. S. J.; Yoon, Y. J.; Yoon, J. Y., *Org.Chem.* **2006**, *71*, 2881-2884.

20. Mokhir, A.; Kramer, R., *Chem. Commun.* **2005**, 2244-2446.

21. Lim, N. C.; Pavlova, S. V.; Bruckner, C., *Inorg. Chem.* **2009**, *48*, 1173-1182.

22. Xu, Z.; Baek, K. -.H; Kim, H. N.; Cui, J.; Qian, X.; Spring, D. R.; Shin, I.; Yoon, J., *J. Am. Chem. Soc.* **2010**, *132*.

23. Diebler, H.; Eigen, M.; Ilgenfritz, G.; Maass, G.; Winkler, R., *Pure Appl. Chem.* **1969**, *20*, 93-115.

3 FerrousBright: Design and Construction of a New Fluorescence Turn-on Probe for Fe^{2+}

3.1 Introduction

Given the need for studying intracellular concentrations of Fe^{2+} in cells[1] we initiated the synthesis of FerrousBright, a potential fluorescence turn-on sensor. Tetramethylboron dipyrromethene (BODIPY) derivatives contain donor and acceptor moieties with differing redox potentials which provide the driving force for PeT.[2, 3] These systems are amenable to synthetic modifications and can be effectively turned as off-on PeT switches for use in metal ion sensing. This chapter outlines and discusses the synthetic and photophysical strategies, used in the construction of FerrousBright, a potential fluorescence turn-on sensor for Fe^{2+} ions.

3.2 Results and Discussion

FerrousBright (Fig. 3.1) consists of a 3,3′,5,5′-tetramethylboron-dipyromethene (BODIPY) fluorophore appended with a tetrapyridyl-diamine receptor. This ligand contains 6 nitrogen donor atoms and is analogous to tetrakis *N,N,N′N′*(2-pyridylmethyl)-propylenediamine (TPTN) (Fig. 3.1). TPTN typically forms tight binding low spin octahedral complexes with transition metals, especially Fe^{2+}.[4-6] Since TPTN contains nitrogen donor atoms, we hypothesized that modifying the phenyl ring to achieve a similar structure would not only provide similar metal binding properties but also a weakly emissive species. Upon metal binding, the PeT process will be interrupted and the fluorescence signal will be restored.

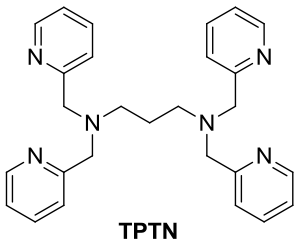

TPTN

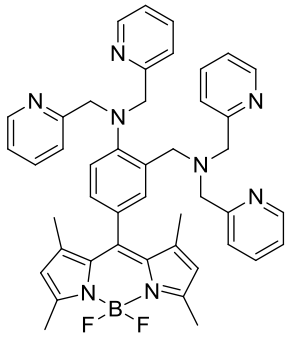

FerrousBright

Figure 3.1 Structure of TPTN and FerrousBright.

Previous report indicated that a Ni^{2+} diamagnetic complex did not quench the emission of a BODPIY fluorphore.[7] On the basis of inefficient electron transfer from the diamagnetic metal complex to the fluorophore, we hypothesized that a low spin Fe^{2+} complex would behave similarly. The larger Δ_o present in the low spin complex may

serve to lower the fully occupied t_{2g} orbital relative to the HOMO of the excited fluorophore, resulting in inefficient electron transfer (Fig. 3.1).

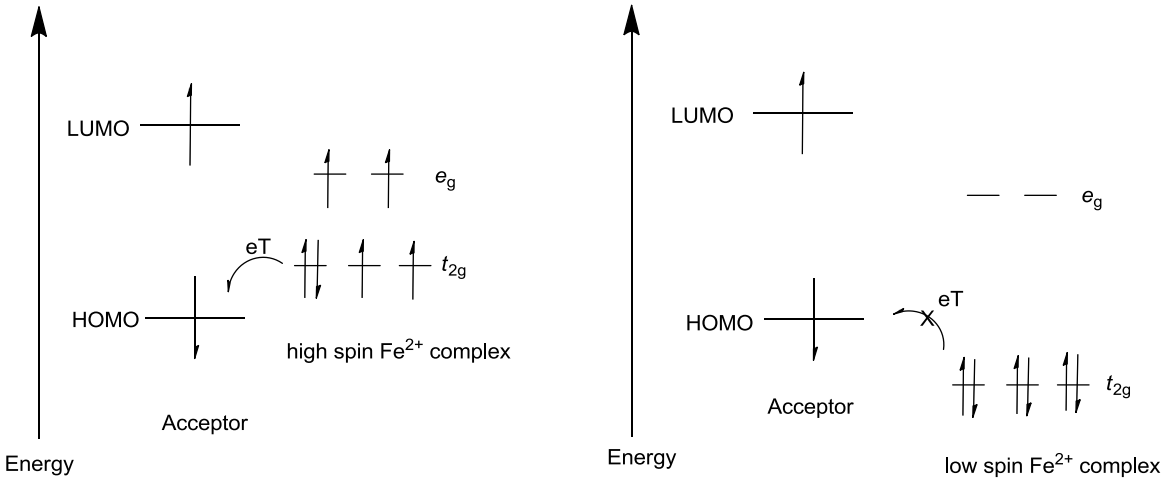

Figure 3.2 Frontier molecular orbital diagram depicting interactions between metal center and fluorophore.

To assess the spin configuration of the metal center in a rudimentary fashion, we synthesized **3.** Ordinarily the spin state is obtained by determining the magnetic moment of the metal complex. Additionally, UV-vis spectra can also be useful in determining this property of the metal center because TPTN-Fe^{2+} low spin complexes possess an intense MLCT band in the visible region. Compound **3** was also used as a scaffold to construct the BODIPY fluorophore. Different routes were explored in the preparation of this molecule because of the ensuing difficulties encountered while attempting to install the fourth pyridyl arm (Scheme 3.1). Initially we envisioned using **1** to perform reductive amination with 2-pyridine carboxaldehyde to construct **3** in a single step. Only **2** was

produced and isolated even after using up to 4 equivalents of the aldehyde, indicating that steric effects limit alkylation. The synthesis of **1** was accomplished in 2 steps using established procedures. Generally poor yields were obtained when the nitro precursor was reduced in the presence of Pd/C and hydrogen gas at atmospheric pressure. Alternatively, hydrazine hydrate with Pd/C proved to be a better reducing agent and **1** was produced in near quantitative yields.

Nucleophilic substitution of **2** with picolyl chloride resulted in no identifiable products while performing the reaction instead with picolyl bromide hydrobromide salt and potassium carbonate furnished the desired product in good yields. The picolyl bromide salt is more soluble in organic solvents like acetonitrile and can be an effective reagent for alkylating aminobenzene derivatives.

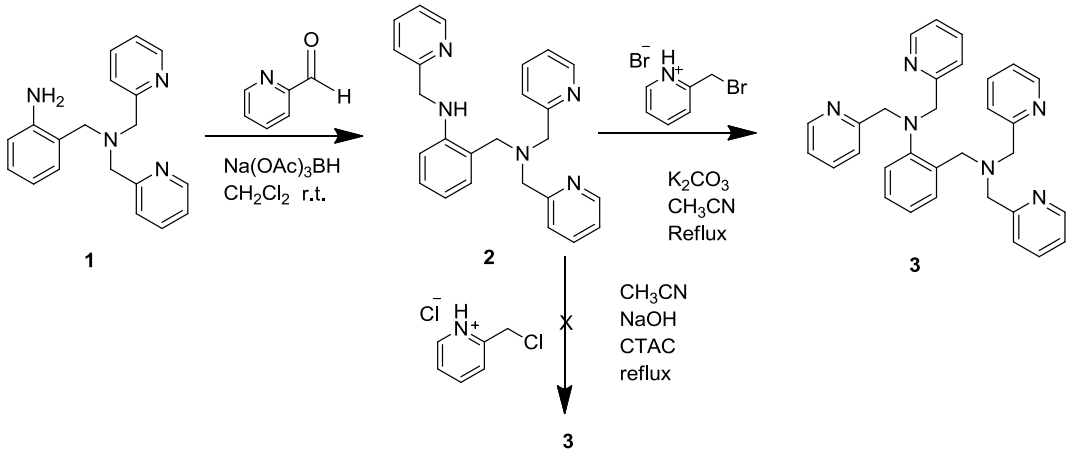

Scheme 3.1 Synthesis of tetrapyridyl ligand.

To examine the binding characteristics of the ligand in solution, a 20 μM sample of **3** was titrated with up to 1.2 equivalents of $FeCl_2$ in methanol. The receptor exhibited a strong absorption band with a λ_{max} at 260 nm. Upon titration with $FeCl_2$, a strong MLCT charge transfer band with λ_{max} at 360 and 460 nm was observed (Fig. 3.2). The extinction coefficient of this band was 9000 M^{-1} cm^{-1} and it compared favorably to the 11000 M^{-1} cm^{-1} obtained for a TPTN-Fe (II) low spin complex.[4] This suggests that FerrousBright will be effective in forming the desired low spin complex with Fe^{2+} ions.

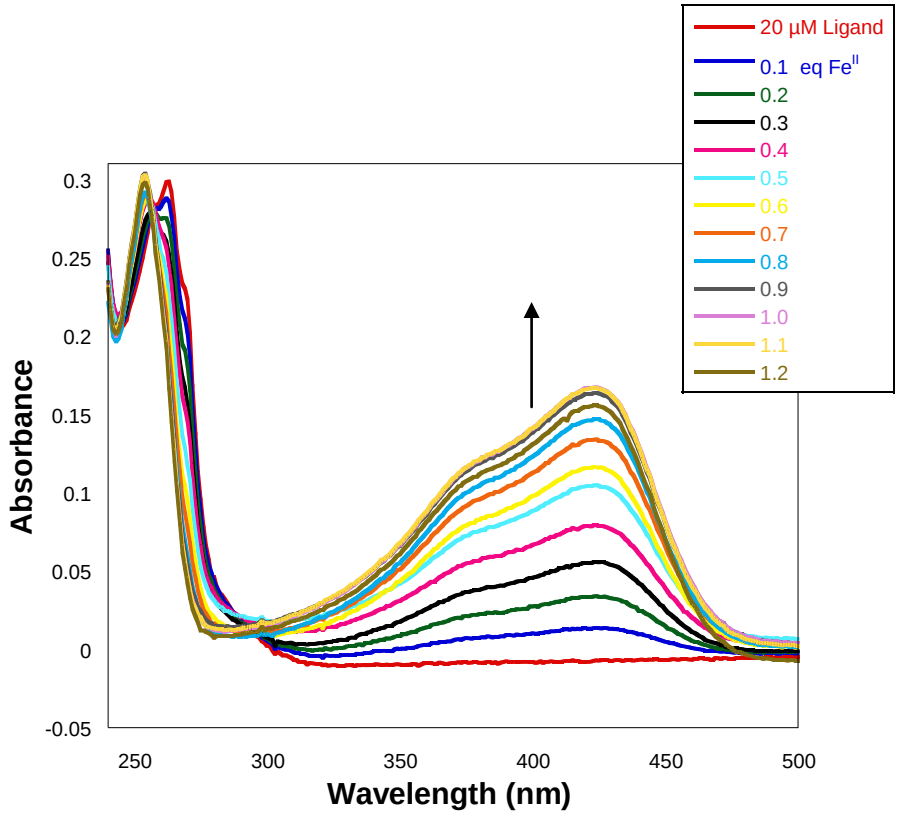

Figure 3.3 UV-Vis titration of tetrapyridyl ligand with $FeCl_2$ in MeOH.

Based on PeT controlled off-on switching in BODIPY derivatives,[2] we posited that **6** should exhibit off-on behavior. Additionally, the same compound could be used to empirically assess whether aniline derivatized donors can be effective quenchers in 3,3′,5,5′-tetramethyl-BODPIY derivatives. To this end, **6** was synthesized and its emission response to Zn^{2+} ions was investigated. The construction of this compound involved attaching a DPA ligand to the BODIPY scaffold, **4** which was prepared according to literature procedure.[8] Reduction using Pd/C in the presence of hydrogen at atmospheric pressure provided **5,** as an orange crystalline material in good yields. Treatment of **5** with approximately 3 equivalents of pyridine carboxaldehyde generated both mono and di-substituted derivatives in a 3:2 ratio. The desired product is a bright orange powder which was intensely emissive in many different organic solvent systems.

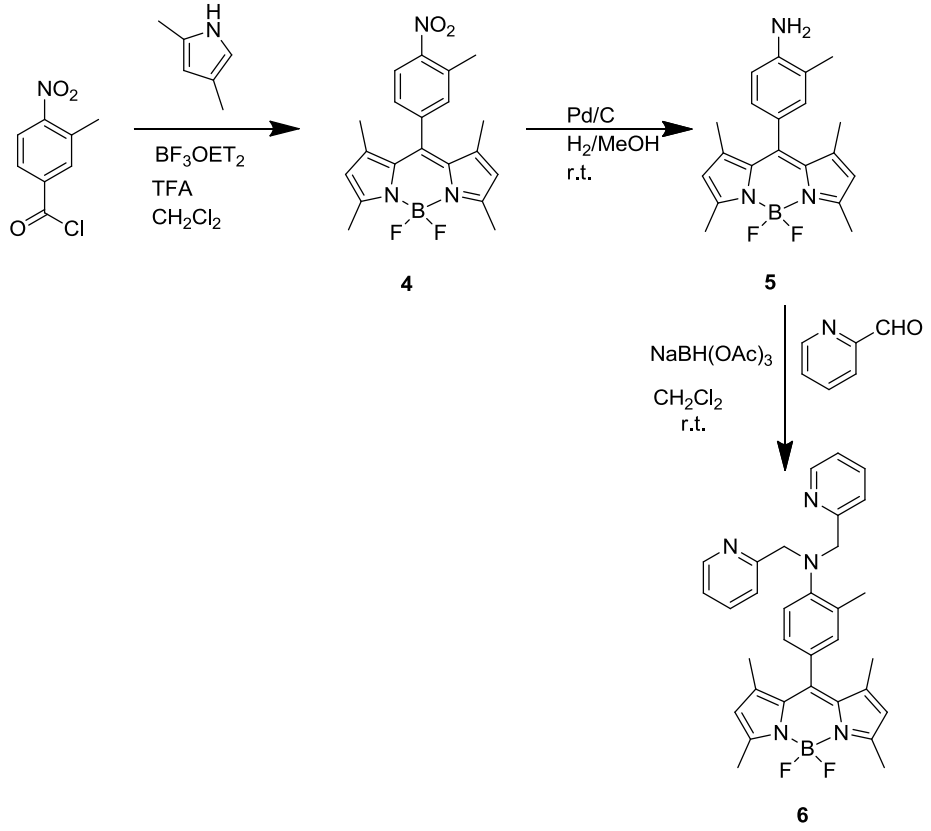

Scheme 3.2 Synthesis of **6**.

To elucidate the emission response, 20 μM of **6** was titrated with up to 300 equivalents of $ZnCl_2$ in methanol (Fig. 3.3). A greater than 4-fold fluorescence enhancement was observed after the addition of up to 6 mM of the metal. The large amount of Zn^{2+} required for the observed fluorescence response was perhaps indicative of the relatively weak interaction between the metal and the DPA ligand, even though this ligand is known to bind to Zn^{2+} with moderate affinity.[9]

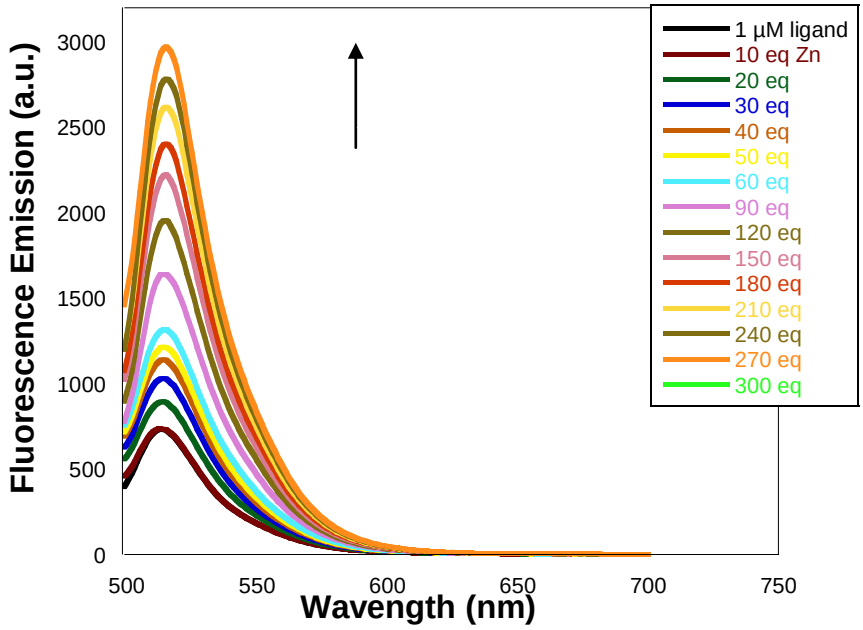

Figure 3.4 Fluorescence emission response of **6** to Zn^{2+}. A 1 μM solution was titrated with 300 μM of $ZnCl_2$ in MeOH. Excitation was performed at 490 nm.

The obtained result indicated that generally di-substituted aniline based BODPIY derivatives with a methylene substituent in the *ortho* position can function as an off-on switch. Since **6** is a PeT-based system the observed fluorescence enhancement can be

attributed to reduction in orbital energy of the donor species (Fig 1.1). This process is facilitated by the coordination of Zn^{2+} ions to the DPA ligand. Given the similarities in structure between **6** and FerrousBright, we expected the former to display analogous switching behavior.

With this information in hand, the synthesis of FerrousBright was undertaken. Even though other methods exist, the preparation of BODPIY dyes usually involves condensation between the corresponding pyrrole and aldehyde.[10] Initially, we envisioned synthesizing this molecule from condensation of the *para*-aldehyde of **3** and the corresponding 2,4 dimethyl pyrrole (Scheme 3.3).

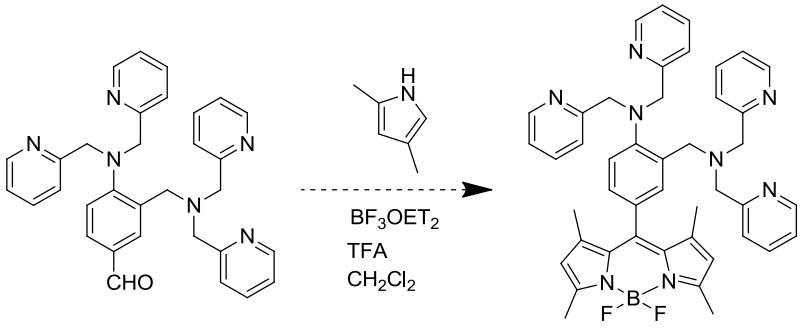

Scheme 3.3 FerrousBright synthesis.

However, preparation of the tetrapyridyl aldehyde proved to be difficult and common formylating reagents failed to provide the desired product. Application of Vilsmeier reaction conditions ($DMF/POCl_3$) to **3** led to multiple products and ^{1} H NMR revealed that none corresponded to the desired product. This was surprising since formylation of dipicolyl aniline proceeded cleanly under analogous conditions. Additionally, Duff reaction conditions (HMTA/AcOH) were effective in transforming the

same substrate into the corresponding *para*-aldehyde; however, this method also proved to be incompatible with **3** due to extensive decomposition.

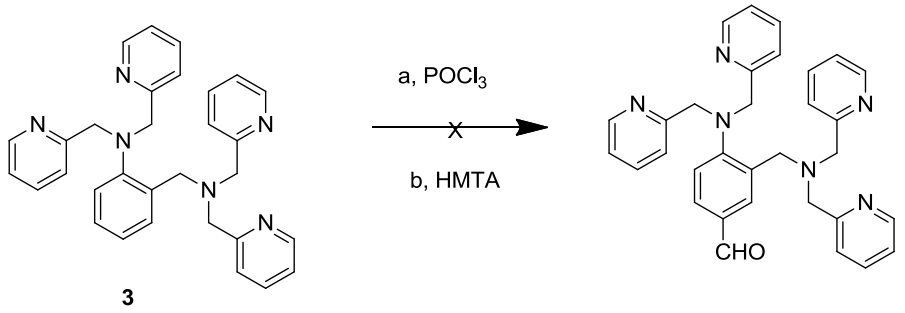

3

Scheme 3.4 Intended synthesis of tetrapyridyl aldeyhyde by formulation of **3**.

As a result, the synthesis was re-engineered and efforts were focused on building the tetrapyridyl ligand off of **4** (Scheme 3.6). The primary objective was to convert the activated methyl group in the *ortho* position of the phenyl ring into the more versatile aldehyde substrate, **8**. *N*,*N*-dimethylformamide dimethyl acetal (DMF-DMA) typically transforms methyl substituents that are *ortho* to an electron withdrawing species into the corresponding enamine.[11-15] This reaction occurs because the nitro-group activates the *ortho*-methyl group toward deprotonation, creating the reactive intermediate shown in Fig. 3.4. As a result, **7** was produced in near quantitative yield when excess DMF-DMA and **4** were combined with DMF at ambient temperature. The product whose structure was confirmed by ^{1}H NMR had a purplish hue, and was non fluorescent. Even though

some enamines are susceptible to hydrolysis under aqueous conditions, **7** proved to be very stable when exposed to similar conditions.

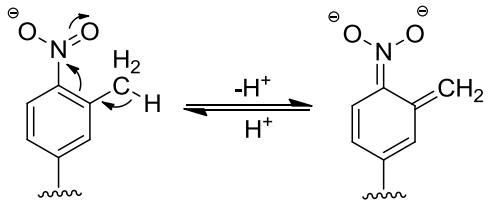

4

Figure 3.5 Illustration depicting activation of methyl group of **4**.

Sodium periodate ($NaIO_4$) oxidized **7** to give the highly fluorescent aldehyde, **8** in approximately 38 % yield. On the other hand, yields obtained for the conversion of other enamines were in the 42- 95 % range.[14] It was suspected that the decrease in yield may be caused by the decomposition of the BODIPY dye as evidenced by the presence of dark colored material which stuck to the base of the chromatography column. Because of the presence of two highly reactive functional groups (aldehyde and nitro), **8** could potentially be a key intermediate for the construction of other BODIPY derivatives with interesting photophysical properties. Aldehydes react favorably with a variety of amines and coupling **8** with dipicolyl amine (DPA) via reductive amination furnished **9** in moderate yields.

The ^{1}H NMR spectrum of **9** (Fig. 3.5) indicates the presence of the pyridyl groups as evidenced by the resonances appearing down-field (in the region 7.0-8.7 ppm). Additionally, the four methylene protons that are adjacent to the pyridine rings are characterized by a singlet, located at ~ 4 ppm. The chemical shifts at ~ 6 and ~6.5 ppm

correspond to pyrrole protons. Surprisingly, they appear as separate resonances. Perhaps asymmetry present in the molecule contributes to this.

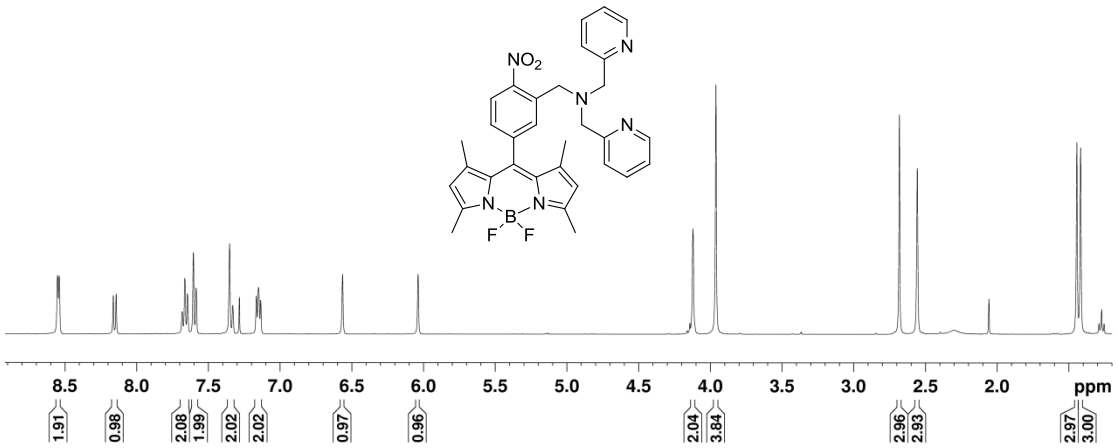

Figure 3.6 ^{1}H NMR spectrum (400 MHz, $CDCl_3$, 25 °C) of **9**.

The aniline derivative **10** was only obtained in 20 % yield while proving difficult to purify. Several different reducing agents were employed but only Pd/C with H_2 at atmospheric pressure resulted in any success. Comparatively, **4** was easily reduced to **5** under similar conditions in quantitative yield. The ease with which the former process occurred seemed to suggest that BODIPY derivatives that contain pyridyl groups are incompatible with this method of reduction. Compound **11** was obtained by routine reductive amination of the amine with 2-pyridine carboxaldehdye in quantities similar to the formation of **9**.

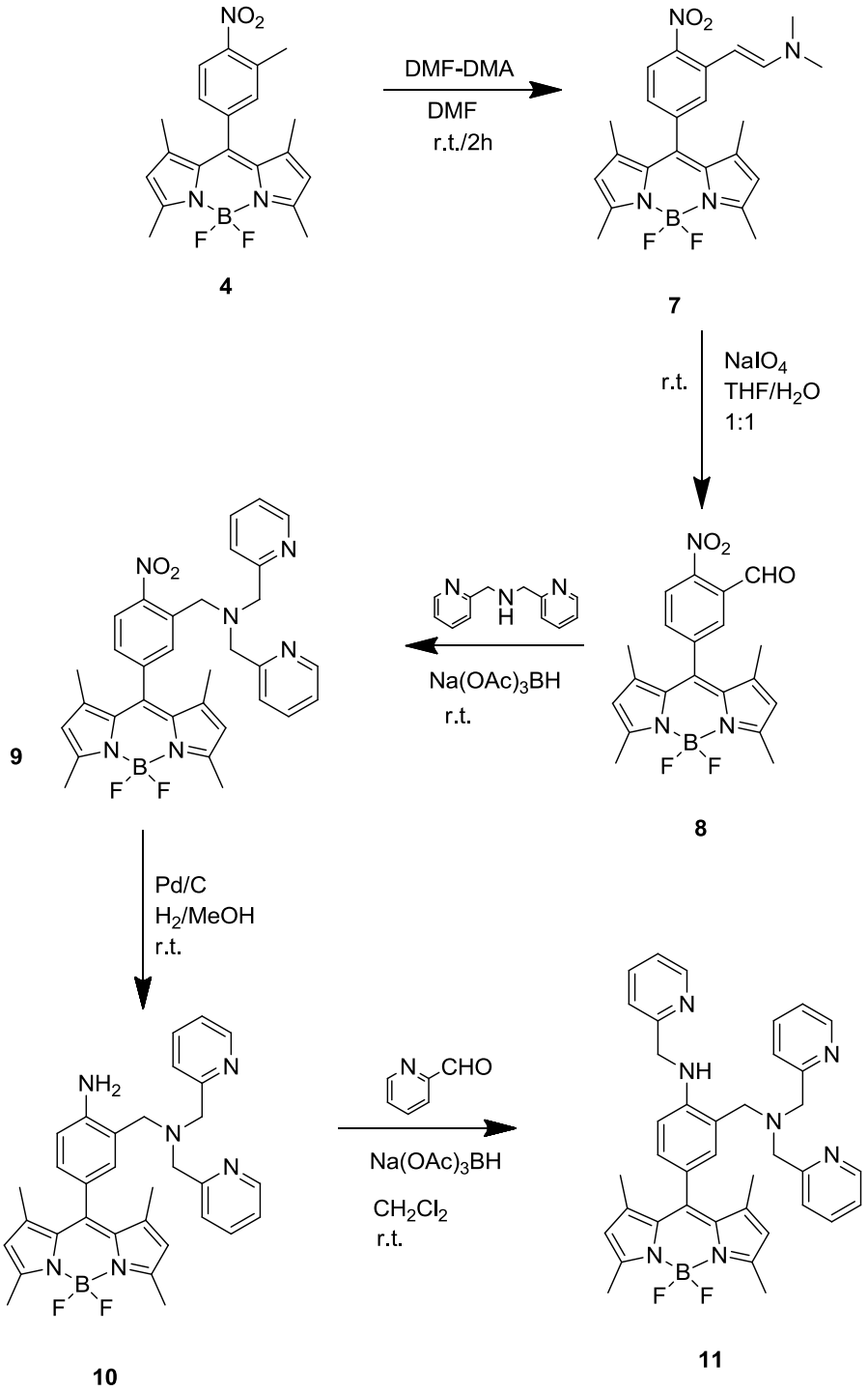

Scheme 3.5 Synthesis of compound **11**.

Installing the fourth pyridyl arm on the aniline nitrogen required overcoming steric crowding caused by the presence of the three pyridyl groups. Schemes 3.6 and 3.7 outline the different routes that were used. The tripyridyl dye (**11**) proved to be incompatible with the reagents that were used to generate **3** as refluxing it with the hydrobromide salt of picolyl bromide and base produced multiple unidentifiable products. Stirring the mixture at room temperature yielded only starting material, while gentle heating led to no observable changes. The relative unreactive nature of **11** appeared not to be borne out of electronic effects. Typically the phenyl rings of the BODIPY fluorophores are spatially perpendicular to the electron-withdrawing indacene moieties. Since the phenyl rings are decoupled from the rest of the molecule, **11** was expected to behave like **3** which undergoes simple alkylation to produce the tetra pyridyl derivative. Given the relative ease with which both tripyridyl derivatives **3** and **11** were formed in comparison to their tetra substituted counterparts, it was evident that steric effects affected the reactivity of these substrates.

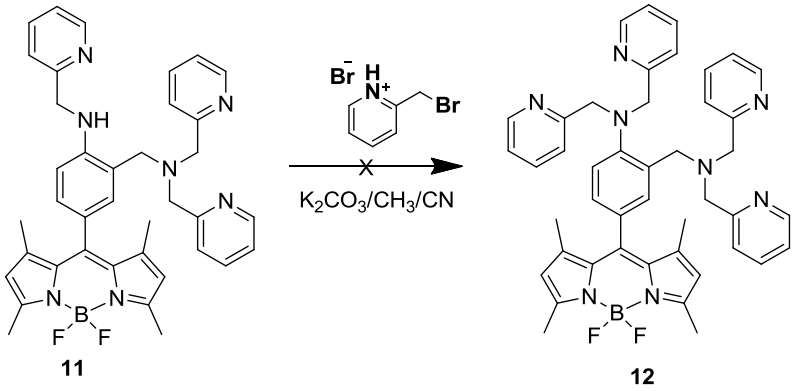

Scheme 3.6 Intended synthesis of Ferrous Bright from tripyridyl and pyridyl bromide.

Based on the general observation of no reaction at mild temperatures and decomposition at higher temperatures, we attempted to make **11** more reactive by deprotonating the aniline hydrogen with sodium hydride. However, this reagent was too harsh for the substrate as decomposition took place. Alternatively, pyridyl mesylate, which in principle is more reactive than the pyridyl bromide, was used (Scheme 3.7). No reaction took place upon heating at modest temperatures, which further confirmed that the reactivity of **11** was limited by steric effects. As previously observed, heating the mixture to elevated temperatures resulted in decomposition.

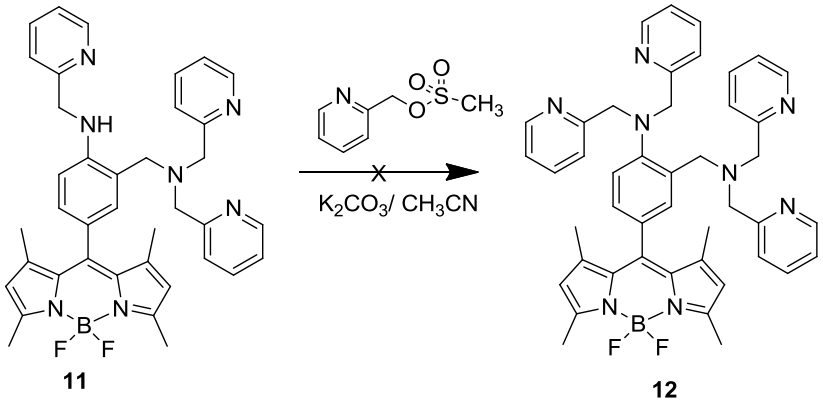

11 **12**

Scheme 3.7 Intended synthesis of Ferrous Bright from tripyridyl and pyridyl mesylate.

3.3 Summary and Future work

Despite the difficulties encountered in completing the final step of the synthesis, we were able to obtain evidence in support of two crucial design aspects of this fluorescence probe. The ligand indeed forms low spin complexes with Fe^{2+} and is suitable to test our hypothesis. In addition, the results obtained from the emission studies of the zinc probe provides experimental evidence that a dipicolyl aniline BODIPY with an electron donating substituent in the *ortho* position does behave as an off-on switch. Constructing FerrousBright through the tripyridyl intermediate (**11**) presented several challenges that proved impossible to overcome. Routes that require reflux temperatures should be avoided since the dye seems to be susceptible to decomposition when heated in the presence of some reagents.

The synthetic route outline below could be a viable approach to the construction of the sensor. Global reduction of **8** with Pd/C in the presence of H_2 would give **13** (Scheme 3.9). The aniline nitrogen could be alkylated with picolylbromide hydrobromide since using 2-pyridine carboxaldehyde at mild temperatures. Bromination of the alcohol with PBr_3 would provide the bromide that should react easily with DPA to furnish the target compound.

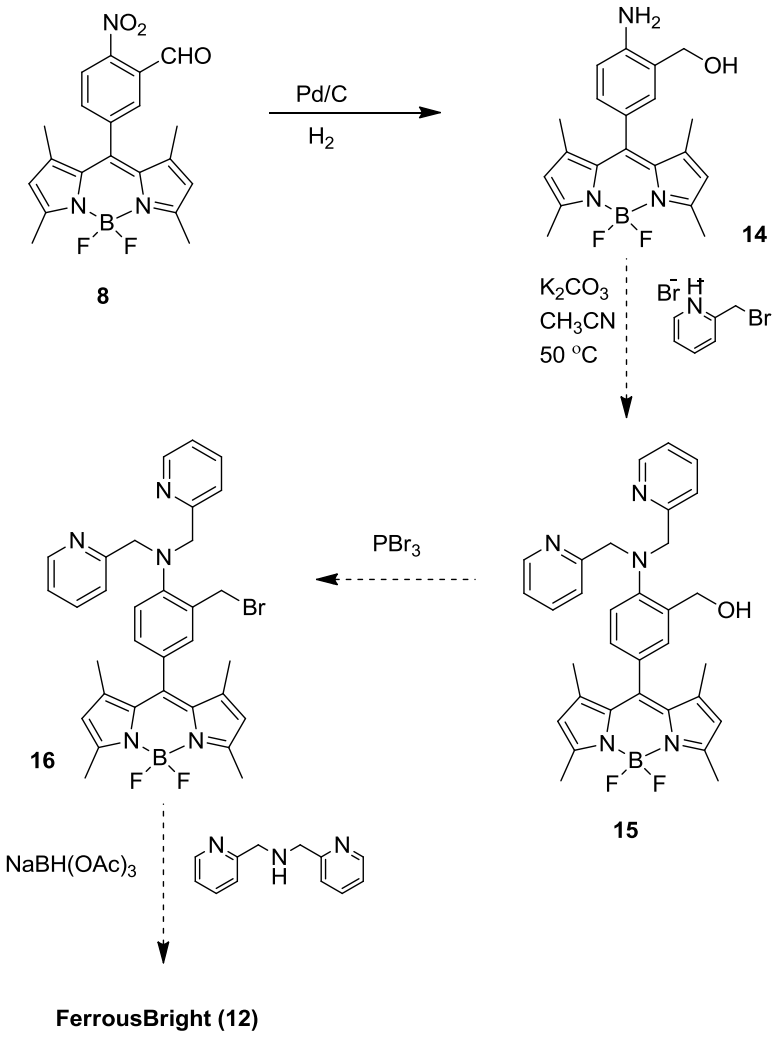

Scheme 3.8 Proposed alternative route to Ferrous Bright.

3.4 Experimental

General procedures. All materials listed below were of research grade or of spectrograde of highest purity available from Acros Organics. Dichloromethane (CH_2Cl_2) and toluene were sparged with argon and dried by passage through a Seca Solvent Purification System. Chromatography and TLC were performed on silica (200-400 mesh) obtained from Silicycle. TLC's were developed using EtOAc/hexanes mixtures. ^{1}H and ^{13}C spectra were recorded using a Bruker 400 MHz NMR instrument. Chemical shifts are reported in ppm relative to tetramethylsilane. IR spectra were recorded on a Nicolet 205 FT-IR instrument. Samples were analyzed as neat. High resolution mass spectra were recorded at the University of Connecticut mass spectrometry facility using an electrospray mass spectrometer operating in negative mode.

Spectroscopy

General methods. The solutions used in these experiments were prepared with spectrophotometric grade solvents. The tetrapyridyl ligand, **3** was dissolved in DMSO to make a 10 mM stock solution. A 6 µL aliquot of this solution was placed in a quartz cuvette and diluted with 3 mL of MeOH to furnish 20 µM for spectroscopic studies. A 10 mM stock solution of $FeCl_2$ was prepared in MeOH. Absorption spectra were recorded on a Cary 50 UV-visible spectrophotometer operated by a PC running a Pentium-IV processor. Spectra were taken at 25 ºC in 1-cm path length cuvettes. Fluorescence spectra were recorded on a Hitachi F-4500 spectrophotometer operated by a PC running a Pentium-IV processor, using the FL solutions 2.0 software. A 150 W Xe lamp provided excitation. A 1 cm path length cuvette was used to acquire spectra. Slit widths are 5 nm

for both excitation and emission, while the photomultiplier tube voltage was set at 700 V unless otherwise stated.

UV-vis experiments with tetrapyridyl ligand and $FeCl_2$. The initial spectrum of a 20 μM solution of the ligand was recorded. Metal ion from 10 mM stock solution was added in 2 μM increments and the spectrum was recorded after each addition. No more changes were observed after the addition of 24 μM of metal ions.

Emission studies compound 6 and $ZnCl_2$. The initial Spectrum of 1 μM of the BODIPY ligand was recorded in MeOH. $ZnCl_2$ was added in 10 μM aliquots up to 300 μM and the spectrum was recorded after each addition.

3.4.1 4,4-Difluoro-8-(4-nitrophenyl-3-methyl)-4-bora-3a,4a-diaza-s-indacene, 4. To a stirred solution of 2,4-dimethyl pyrrole (900 μL, 8.70 mmol) in CH_2Cl_2 (10 mL) was added freshly prepared nitro-2-methyl benzoyl chloride (870 mg, 4.31 mmol). The resulting mixture was stirred at room temperature for 24 h after which triethylamine (3.60 mL, 25.8 mmol) was added. After 5 minutes of stirring, $BF_3.OEt_2$, (4.40 mL, 34.0 mmol) was added to create a purple-brown mixture which was stirred for 1 h. The mixture was washed with saturated $NaHCO_3$ (2 × 10 mL). The organic layers were combined and the solvent was removed by vacuum. Flash chromatography on silica using EtOAc/hexanes 1:10 yielded a bright orange solid (1.00 g, 30.1 %). TLC, R_f = 0.4, (silica, 1:4, EtOAc:hexanes). ^{1}HNMR (400 MHz, $CDCl_3$), δ 8.17 (d, J = 8.2 Hz, 2 H), 7.37 (d, J = 9.1 Hz, 2 H), 6.04 (s, 2 H), 2.70 (s, 3 H), 2.58 (s, 6 H), 1.42 (s, 6 H). ^{13}C NMR (100 MHz, $CDCl_3$) δ 156.8, 149.6, 142.8, 140.5, 138.7, 135.1, 132.9, 130.9, 127.3, 125.9, 122.0, 20.7, 15.0, 14.9. IR (neat, cm^{-1}) 3001.1, 2918.2, 2798.2, 1587.8, 1568.7,

1486.8, 1469.8, 1454.0, 1431.2, 1368.9, 1322.1, 1298.2, 1281.0, 1248.7, 1203.8, 1144.6, 1133.4, 1096.4, 1047.3, 994.4, 984.0, 966.3, 948.2, 931.9, 905.0, 820.0, 657.4. HRMS (−ESI), calcd for $C_{20}H_{21}BF_2N_3O_2^-$ 384.1731; found 384.1700.

3.4.2 4,4-Difluoro-8-(4-nitrophenyl-3-enamine)-4-bora-3a,4a-diaza-s-indacene, 7.

To a stirred solution of **4** (950 mg, 2.47 mmol) in 15 mL of DMF was added DMF-DMA (670 μL, 6.21 mmol). The mixture was stirred for 10 h. Solvent was removed by vacuum to yield a shiny purple solid. The compound was used without further purification in the next step (1.07 g, 99.1%). TLC, R_f = 0.2 (silica, 1:4, EtOAc:hexanes). ^{1}H NMR (400 MHz, $CDCl_3$), δ 8.11 (d, J = 8 Hz, 1 H), 7.37 (d, J = 8 Hz, 2 H), 7.25 (d, J = 12 Hz, 1 H), 6.32 (s, 1 H), 5.94 (d, J = 12 Hz, 1 H), 5.86 (s, 1 H), 3.08 (s, 6 H), 2.66 (s, 3 H), 2.52 (s, 3H), 1.40 (s, 3 H), 1.35 (s, 3 H). ^{13}C NMR (100 MHz, $CDCl_3$) δ 198.83, 160.04, 150.47, 149.10, 145.99, 143.47, 142.05, 134.49, 134.12, 133.36, 133.17, 129.83, 128.46, 125.35, 118.23, 117.82, 90.16, 20.76, 15.49, 14.35. HRMS (−ESI), calcd for $C_{32}H_{32}BF_2N_5^-$ 536.2803; found 536.2789

3.4.3 4,4-Difluoro-8-(4-nitrophenyl-3-aldehyde)-4-bora-3a,4a-diaza-s-indacene,

8. The enamine (910 mg, 2.00 mmol) was dissolved in a 1:1 mixture of THF/H_2O (10 mL). Sodium periodate (1.30 g, 12.0 mmol) was added and the mixture was stirred for 6 h. The heterogeneous mixture was filtered by vacuum and the white solid was washed with EtOAc (2 × 10 mL). The filtrate were combined, washed with $NaHCO_3$ (2 × 10 mL) and dried over Na_2SO_4. Solvent was removed by vacuum and the dark green residue was purified on silica by flash chromatography using EtOAc:hexanes, 1:4 to yield a red solid which appears green due to fluorescence (357 mg, 45.1 %). TLC, R_f = 0.3, (silica, 1:4, EtOAc:hexanes). ^{1}H NMR (400 MHz, $CDCl_3$), δ 10.28 (s, 1 H), 8.21 (d, J =

9.1 Hz, 1 H), 7.40 (d, *J* = 8.6 Hz, 2 H), 6.81 (s, 1 H) 6.30 (s, 1 H), 2.72 (d, *J* = 4.5 Hz, 2 H), 1.54 (s, 3 H), 1.46 (s, 3 H). ^{13}C NMR (100 MHz, $CDCl_3$) δ 184.6, 184.6, 167.4, 150.0, 149.2, 144.4, 141.0, 139.1, 137.7, 135.6, 135.4, 132.5, 127.0, 126.2, 126.1, 120.38, 20.7, 16.0, 15.7, 14.8, 14.4. IR (neat, cm^{-1}) 2926.8, 1650.8, 1610.8, 1589.4, 1550.8, 1519.1, 1477.2, 1436.0, 1389.1, 1334.4, 1310.2, 1275.5, 1211.6, 1185.2, 1137.1, 1173.0, 1079.8, 1048.2, 938.0, 918.9, 878.8, 768.7, 740.8, 706.5, 658.6. HRMS (−ESI), calcd for $C_{20}H_{19}BF_2N_3O_3^-$ 398.1491; found 398.1506

3.4.4 4,4-Difluoro-8-(4-nitrophenyl-3-N,N-bispyridyl)-4-bora-3a,4a-diaza-s-indacene, 9. The aldehyde (1.30 g, 3.80 mmol) and dipicolylamine (910 mg, 4.56 mmol) were combined in CH_2Cl_2 (20 mL) and $NaBH(OAc)_3$ (1.00 g, 5.00 mmol) was added. The mixture was stirred for 24 h at room temperature. After the addition of water (10 mL) the organic layer was separated, collected and dried over Na_2SO_4. Solvent was removed by vacuum and the residue was purified by flash chromatography on alumina by initially using EtOAC:hexanes 1:3 followed by 2:3 EtOAc:hexanes to yield a dark red solid (890 mg, 45.3 %). TLC, R_f = 0.25 (alumina, 1:4 EtOAc:hexanes). ^{1}H NMR (400 MHz, $CDCl_3$), δ 8.55 (d, *J* = 4 Hz, 2 H), 8.16 (d, *J* = 8 Hz, 1 H), 7.68 (t, *J* = 8 Hz, 2 H), 7.60 (d, *J* = 8 Hz, 2 H), 7.35 (d, *J* = 8 Hz, 2 H), 7.16 (t, *J* = 8 Hz, 2 H), 6.56 (s, 1 H) 6.04 (s, 1 H), 4.12 (s, 2 H), 3.96 (s, 4 H), 2.69 (s, 3 H), 2.54 (s, 3 H), 1.44 (s, 3 H), 1.41 (s, 3 H). ^{13}C NMR (100 MHz, $CDCl_3$) δ 159.5, 158.3, 157.9, 149.6, 149.4, 143.6, 142.3, 140.4, 139.2, 136.7, 135.2, 132.9, 127.2, 125.9, 122.8, 122.4, 122.2, 120.4, 60.9, 47.2, 20.7, 15.2, 15.1, 14.9. IR (neat, cm^{-1}) 2914.5, 1588.9, 1568.5, 1540.5, 1507.0, 1460.3, 1431.0, 1410.2, 1345.1, 1305.9, 1265.1, 1221.5, 1186.7, 1144.3, 1105.3, 1066.8, 1048.7,

978.5, 954.6, 910.2, 876.7, 828.9, 815.4, 759.1, 740.3, 696.4. HRMS (−ESI), calcd for $C_{32}H_{32}BF_2N_6O_2^-$ 581.2653; found 581.2660

3.4.5 4,4-Difluoro-8-(4-aminophenyl-3-N-N-bispyridyl)-4-bora-3a,4a-diaza-s-indacene, 10. To a stirred solution of **9** (550 mg, 0.948 mmol) in 1:1 MeOH/CH_2Cl_2 (10 mL) was added Pd/C (101 mg, 10 mol %). The mixture was stirred under H_2 at atmospheric pressure for 18 h, after which it was filtered over Celite. Solvent was removed by vacuum and the residue was purified by flash chromatography on alumina using 1:99 MeOH/CH_2Cl_2 to yield a dark red sticky solid (140 mg, 20.1 %). TLC, R_f = 0.2 (alumina, 1:19 MeOH/CH_2Cl_2). ^{1}H NMR (400 MHz, $CDCl_3$), δ 8.54 (d, J = 4.7 Hz, 2 H), 7.65-7.61 (m, 4 H), 7.15-7.11 (m, 2 H), 6.93-6.85 (m, 2 H), 6.78 , 6.50 (s, 1 H), 5.99 (s, 1 H), 4.11 (s, 2 H), 3.96 (s, 4 H), 2.5 (s, 3 H), 2.21 (s, 3 H), 1.52 (s, 3 H), 1.50 (s, 3 H).

3.4.6 4,4-Difluoro-8-(4-N-pyridyl-phenyl-3-N,N-bispyridyl)-4-bora-3a,4a-diaza-s-indacene (Tripyridyl-BODIPY), 11 The aniline (70.0 mg, 0.127 mmol) and 2-pyridine carboxaldehyde (28.6 mg, 0.267 mmol) were combined in CH_2Cl_2 (5 mL) and $NaBH(OAc)_3$ (94.2 mg, 0.444 mmol) was added. The mixture was stirred for 24 h at room temperature. After the addition of water (5 mL), the organic layer was separated, collected and dried over Na_2SO_4. Solvent was removed by vacuum and the residue was purified by flash chromatography on alumina using EtOAC:hexanes 1:10 and 2:5 EtOAc:hexanes to yield a dark red solid (40.7 mg, 50.1 %). TLC, R_f = 0.3, (alumina 1:1, EtOAc:hexanes). ^{1}H NMR (400 MHz, $CDCl_3$), δ 8.65 (d, J = 4.6 Hz, 1 H), 8.54 (d, J = 4.6 Hz, 2 H), 7.72 -7.61 (m, 5 H), 7.35 (d, J = 8.2 Hz, 1 H), 7.26 (t, J = 6.0 Hz, 1 H), 7.18 (t, J = 5.0 Hz, 3 H), 6.97 (d, J = 7.0 Hz, 1 H), 6.51 (s, 1 H), 5.98 (s, 1 H), 5.05 (s, 1 H), 4.55 (s, 2 H), 4.12 (s, 2 H), 3.97 (s, 4 H), 2.54 (s, 3 H), 2.30 (s, 3 H), 1.52 (s, 3 H), 1.49

(s, 3H) IR (neat, cm^{-1}) 3385.1, 2920.9, 1734.4, 1610.8, 1589.2, 1569.7, 1539.6, 1506.4, 1432.2, 1407.7, 1350.4, 1307.9, 1261.4, 1187.8, 1148.0, 1116.2, 1078.2, 1045.3, 975.2, 907.0, 811.7, 761.3.

3.4.7 2-{[Bis(pyridine-2-ylmethyl)amino]methyl}-N-(pyridine-2-ylmethyl)aniline, 2.

The aniline, **1** (230 mg, 0.760 mmol), 2- pyridine carboxaldehyde, (120 mg, 1.10 mmol) were dissolved in dichloromethane (10 mL). To this solution was added $NaBH(OAc)_3$ (2.30 mg, 1.10 mmol). The mixture was stirred at room temperature for 12 h and water (10 mL) was added, the organic layer collected and dried over Na_2SO_4. Solvent was removed by vacuum and the residue was purified by flash chromatography on alumina using 99:1 DCM:MeOH to yield a light yellow solid (0.24 g, 80). TLC, R_f = 0.4, (alumina 9:1, CH2Cl2:MeOH). ^{1}H NMR (400 MHz, $CDCl_3$), δ 8.67 (d, J = 5.2 Hz, 1 H), 8.52 (d, J = 4.3 Hz, 2 H), 7.58 (m, 3 H), 7.45 (d, J = 8.0 Hz, 2 H), 7.33 (d, J = 8.0 Hz, 1 H), 7.19 (t, J = 7.2 Hz, 1 H), 7.13 – 7.04 (m, 4 H), 6.62 (t, J = 7.2 Hz, 1 H), 6.45 (d, J = 8.2 Hz, 1 H), 4.61 (s, 2 H), 3.87 (s, 4 H), 3.76 (s, 2 H). ^{13}C NMR (100MHz, $CDCl_3$) δ 160.7, 159.5, 149.3, 149.3, 148.1, 136.8, 136.6, 131.3, 129.0, 123.6, 122.2, 122.0, 121.5, 116.2, 110.4, 60.3, 58.7, 49.5. IR (neat, cm^{-1}) 3292.6, 3003.6, 2921.6, 2802.6, 1588.3, 1568.0, 1531.4, 1470.8, 1454.8, 1429.3, 1378.3, 1368.1, 1357.4, 1331.2, 1315.2, 1289.8, 1275.1, 1254.2, 1210.2, 1118.5, 1099.0, 1048.9, 991.9, 977.4, 931.1, 889.4, 857.1, 841.2, 751.4. HRMS (−ESI), calcd for $C_{25}H_{26}N_5^-$ 396.2188; found 396.2118.

3.4.8 2-{[Bis(pyridine-2-ylmethyl)amino]methyl}-N,N-bis(pyridin-2-ylmethyl) aniline, 3.

The tripyridyl, **2** (1.40 g, 3.50 mmol) was combined with picolylbromide hydrobromide, (1.21 g, 4.62 mmol), potassium carbonate, (4.81 g, 35.2 mmol), and sodium iodide, (3.72 mg, 20.1 mol %) in acetonitrile. The mixture was refluxed for 48 h

after which it was filtered and the residue was washed with acetonitrile (5 mL). The filtrate were combined and the solvent was removed by vacuum. The residue was purified on alumina using 4:1 CH_2Cl_2:EtOAC to yield light brown oil (1.72 g, 50.3 %). TLC, R_f = 0.2 (alumina, 9:1, CH_2Cl_2:MeOH). ^{1}HNMR (400 MHz, $CDCl_3$), δ 8.52 (d, J = 5.3 Hz, 2 H), 8.49 (d, J = 4.8 Hz, 2 H), 7.86 – 7.84 (m, 1 H), 7.68 (t, J = 7.6 Hz, 2 H), 7.61 (d, J = 7.4 Hz, 2 H), 7.57 (t, J = 7.2 Hz, 2 H), 7.39 (d, J = 8.0 Hz, 2 H), 7.16 (t, J = 5.8 Hz, 2 H), 7.09 (t, J = 3.9 Hz, 5 H), 4.31 (s, 4 H), 3.95 (s, 2 H) 3.82 (s, 4 H). ^{13}C NMR (100 MHz, $CDCl_3$) δ 160.1, 158.7, 149.5, 149.3, 149.2, 136.7, 136.6, 134.8, 129.5, 124.3, 122.9, 122.8, 122.8, 122.2, 122.2, 60.7, 53.7. IR (neat, cm^{-1}) 3001.1, 2918.2, 1587.8, 1568.7, 1486.8, 1469.8, 1454.03, 1431.2, 1368.9, 1322.1, 1298.2, 1281.0, 1248.7, 1203.8, 1144.6, 1133.4, 1096.6, 1047.3, 994.4, 984.0, 966.9, 948.2, 931.9, 820.0, 759.6, 732.4, 715.9, 657.4. HRMS (−ESI), calcd for $C_{31}H_{31}N_6^-$ 487.2610; found 487.2626.

3.4.9 4,4-Difluoro-8-(4-aminophenyl-3-methyl)-4-bora-3a,4a-diaza-s- indacene, 5.

To a stirred solution of **4** (1.00 g, 2.61 mmol) 1:1 MeOH/CH_2Cl_2 (10 mL) was added Pd/C (270 mg, 10.0 mol %). The mixture was stirred under H_2 at atmospheric pressure for 4 h, after which it was filtered over Celite. The solvent was removed by vacuum to yield an orange solid (822 mg, 82.2 %) which was used in the next step without further purification. TLC R_f = 0.2 (silica, 1:3 EtOAc:hexanes) ^{1}H NMR (400 MHz, $CDCl_3$), δ 6.94 (s, 1 H), 6.92 (s, 1 H), 6.90 (s, 1 H), 6.79 (s, 1 H), 6.77 (s, 1 H), 3.80 (s, 2 H), 2.56 (s, 6 H), 2.22 (s, 3 H), 1.50 (s, 6 H). ^{13}C NMR (100MHz, $CDCl_3$) δ 155.0, 145.4, 143.4, 132.3, 130.1, 126.8, 125.0, 123.1, 121.1, 115.5, 17.5, 14.9, 14.79. IR (neat, cm^{-1}) 3497.8, 3404.5, 2923.4, 1625.7, 1538.4, 1495.2, 1464.4, 1405.4, 1361.9, 1298.5, 1262.7, 1189.8,

1154.4, 1084.1, 1053.8, 968.1, 839.5, 816.5, 761.6, 734.2, 714.7. HRMS (−ESI), calcd for $C_{20}H_{22}BF_2N_3^-$ 354.1957; found 354.1932.

3.5.0 4,4-difluoro-8-(4-N,N-dipocolylaminophenyl-3-methyl)-4-bora-3a,4a-diaza-s-indacene 6. The aniline, (640 mg 1.81 mmol), 2-pyridine carboxaldehyde, (681 mg, 6.30 mmol) were dissolved dichloromethane (15 mL). To this solution was added $NaBH(OAc)_3$ (1.34 g, 6.30 mmol). The mixture was stirred at room temperature for 12 h. Water (6 mL) was added and the organic layer was collected and dried over Na_2SO_4. Solvent was removed by vacuum and the residue was purified by flash chromatography on alumina using EtOAc:hexanes 1:4 to yield **9** as a bright orange solid (436 mg, 45.1 %) TLC, R_f = 0.3 (alumina, 2:3 EtOAc:hexanes). ^{1}H NMR (400 MHz, $CDCl_3$), δ 8.54 (d, J = 4.2 Hz, 2 H), 7.59 (t, J = 8.0 Hz, 2 H), 7.34 (d, J = 8.4 Hz, 2 H), 7.16 (t, J = 6.2 Hz, 2 H), 7.05 (d, J = 7.7 Hz, 2 H), 6.88 (d, J = 9.1 Hz, 2 H), 4.50 (s, 4 H), 2.59 (s, 6 H), 2.47 (s, 3 H), 1.26 (s, 6 H). ^{13}C NMR (100MHz, $CDCl_3$) δ 158.4, 155.3, 149.3, 149.2, 143.19, 142.2, 136.5, 135.0, 131.8, 130.7, 130.2, 126.0, 123.6, 122.9, 122.3, 121.2, 60.0, 18.8, 14.8, 14.6. IR (neat, cm^{-1}) 2922.7, 1590.3, 1541.0, 1508.7, 1436.9, 1409.2, 1362.7, 1348.4, 1305.6, 1263.0, 1184.8, 1153.8, 1117.5, 1085.6, 972.4, 942.5, 879.4, 838.3, 817.7, 770.8, 744.5, 722.4, 653.8. HRMS (−ESI), calcd for $C_{23}H_{26}BF_2N_4O_2^-$ 439.2121; found 439.2126.

References

1. Domaille, D. W.; Que, E. L.; Chang, C. J., *Nat. Biol. Chem.* **2008**, *4*, 168-174.

2. Sunahara, H.; Urano, Y.; Kojima, H.; Nagano, T., *J. Am. Chem. Soc.* **2007**, *129*, 5597-5604.

3. Turfan, B.; Akkaya, E. U., *Org. Lett.* **2002**, *4*, 2857-2859.

4. McCusker, J. K.; Walda, K. N.; Dunn, R. C.; Magde, D.; Hendrickson, D. N., *J. Am. Chem. Soc.* **1993**, *115*, 298-307.

5. Toftlund, H.; Yde-Andersen, S., *Acta. Chem. Scand.* **1981**, *35*, 575-585.

6. Pandiyan, T.; Consuela-Estrada, V. M.; Moreno-Esparza, R.; Ruiz-Ramirez, L., *Inorg. Chimi. Acta.* **2003**, *343*, 79-89.

7. Dodani, S. C.; Qiwen, H.; Chang, C. J., *J. Am. Chem. Soc.* **2009**, *131*, 18020-18021.

8. Ziesel, R.; Bonardi, L.; Retailleau, P.; Ulrich, G., *J. Org. Chem.* **2006**, *71*, 3093-3102.

9. Gwizdala, C.; Kennedy, D. P.; Burdette, S. C., *Chem. Commun.* **2009**, 6967-6969.

10. Jiao, L.; Yu, C.; Liu, M.; Wu, Y.; Cong, K.; Meng, T.; Wang, Y.; Hao, E., *J. Org. Chem.* **2010**, *75*, 6035-6038.

11. Siu, J.; Baxendale, I. R.; Ley, S. V., *Org. Biomol. Chem.* **2004**, *2*, 160-167.

12. Arai, E.; Tokuyama, H. J.; Linsell, M. S.; Fukuyama, T., *Tetrahedron Lett.* **1998**, *39*, 71-74.

13. Gupton, J. T.; Lizzi, M. J.; Polk, D., *Synth. Commun.* **1982**, *12*, 939-946.

14. Valentino, M. G.; Coe, J. W., *Tetrahedron Lett.* **1994**, *35*, 219-222.

15. Robertson, A. A. B.; Botting, N. P., *Tetrahedron* **1999**, *55*, 13269-13284.